



Composition of hydrothermal fluids and mineralogy of associated chimney material on the East Scotia Ridge back-arc spreading centre

Rachael H. James^{a,*}, Darryl R.H. Green^a, Michael J. Stock^{a,1}, Belinda J. Alker^a,
Neil R. Banerjee^b, Catherine Cole^{c,2}, Christopher R. German^d,
Veerle A.I. Huvenne^a, Alexandra M. Powell^b, Douglas P. Connelly^a

^a National Oceanography Centre, Southampton, European Way, Southampton SO14 3ZH, UK

^b Department of Earth Sciences, Western University, London, Ontario N6A 3K7, Canada

^c Ocean and Earth Science, National Oceanography Centre, Southampton, University of Southampton, European Way, Southampton SO14 3ZH, UK

^d Geology and Geophysics, Woods Hole Oceanographic Institution, 266 Woods Hole Rd., Woods Hole, MA 02543-1050, USA

Received 15 November 2013; accepted in revised form 18 April 2014; available online 6 May 2014

Abstract

The East Scotia Ridge is an active back-arc spreading centre located to the west of the South Sandwich island arc in the Southern Ocean. Initial exploration of the ridge by deep-tow surveys provided the first evidence for hydrothermal activity in a back-arc setting outside of the western Pacific, and we returned in 2010 with a remotely operated vehicle to precisely locate and sample hydrothermal sites along ridge segments E2 and E9. Here we report the chemical and isotopic composition of high- and low-temperature vent fluids, and the mineralogy of associated high-temperature chimney material, for two sites at E2 (Dog's Head and Sepia), and four sites at E9 (Black & White, Ivory Tower, Pagoda and Launch Pad). The chemistry of the fluids is highly variable between the ridge segments. Fluid temperatures were ~350 °C at all vent sites except Black & White, which was significantly hotter (383 °C). End-member chloride concentrations in E2 fluids (532–536 mM) were close to background seawater (540 mM), whereas Cl in E9 fluids was much lower (98–220 mM) indicating that these fluids are affected by phase separation. Concentrations of the alkali elements (Na, Li, K and Cs) and the alkaline earth elements (Ca, Sr and Ba) co-vary with Cl, due to charge balance constraints. Similarly, concentrations of Mn and Zn are highest in the high Cl fluids but, by contrast, Fe/Cl ratios are higher in E9 fluids ($3.8\text{--}8.1 \times 10^{-3}$) than they are in E2 fluids ($1.5\text{--}2.4 \times 10^{-3}$) and fluids with lowest Cl have highest Cu. Although both ridge segments are magmatically inflated, there is no compelling evidence for input of magmatic gases to the vent fluids. Fluid δD values range from 0.2‰ to 1.5‰, pH values (3.02–3.42) are not especially low, and F concentrations (34.6–54.4 μM) are lower than bottom seawater (62.8 μM). The uppermost sections of conjugate chimney material from E2, and from Ivory Tower and Pagoda at E9, typically exhibit inner zones of massive chalcopyrite enclosed within an outer zone of disseminated sulphide, principally sphalerite and pyrite, in an anhydrite matrix. By contrast, the innermost part of the chimneys that currently vent fluids with lowest Cl (Black & White and Launch Pad), is dominated by anhydrite. By defining and assessing

* Corresponding author. Address: Ocean and Earth Science, National Oceanography Centre, Southampton, University of Southampton, European Way, Southampton SO14 3ZH, UK. Tel.: +44 2380599005.

E-mail address: R.H.James@soton.ac.uk (R.H. James).

¹ Current address: Department of Earth Sciences, University of Oxford, South Parks Road, Oxford OX1 3AN, UK.

² Current address: School of Geography & Geosciences, University of St Andrews, North Street, St Andrews KY16 9AL, UK.

the controls on the chemical composition of these vent fluids, and associated mineralisation, this study provides new information for evaluating the significance of hydrothermal processes at back-arc basins for ocean chemistry and the formation of seafloor mineral deposits.

© 2014 The Authors. Published by Elsevier Ltd. This is an open access article under the CC BY license (<http://creativecommons.org/licenses/by/3.0/>).

1. INTRODUCTION

Several decades of exploration have resulted in the detection of hydrothermal vents at numerous mid-ocean ridges sites, and in rather fewer back-arc basins (e.g. [Ishibashi and Urabe, 1995](#); [Von Damm, 1995](#); [German and Von Damm, 2003](#)). For the most part, sampling of back-arc basin hydrothermal systems has been restricted to sites in the western Pacific (e.g. [Gamo et al., 2006](#)). The first evidence for hydrothermal activity in a back-arc setting in the South Atlantic, was reported for the East Scotia Ridge (ESR) by [German et al. \(2000\)](#), who found enrichments in concentrations of particulate material and dissolved manganese in the water column above the ridge crest at two locations. Evidence for hydrothermal activity on the Bransfield Strait back-arc spreading ridge, including elevated levels of dissolved manganese in the water column and chimney fragments recovered by dredging, was subsequently reported by [Klinkhammer et al. \(2001\)](#). However, activity in this region may be ephemeral ([Aquilina et al., 2013](#)).

In the austral summer of 2009, tethered camera operations carried out from RRS *James Clark Ross* on cruise JR224 returned images of black smoker chimneys as well as areas of diffuse venting on two segments of the ESR ([Rogers et al., 2012](#)). As it was not possible to sample these systems on this cruise, we returned to these sites in early

2010 with the remotely operated vehicle (ROV) *ISIS* on RRS *James Cook* cruise JC42. *ISIS* was used to take samples of both high- and low-temperature vent fluids, the associated vent fauna, vent chimneys and other mineral deposits, and for detailed bathymetric, visual and geophysical surveys. Analysis of the faunal assemblage reveals that the vents are inhabited by new, undescribed species of anomuran crab, colepadid barnacle, lepetodrilid and pellospiroid gastropods, actinostolid anemones, and a stichasterid seastar, which represent a new province of vent biogeography ([Rogers et al., 2012](#)).

Here we report the first results of shipboard and shore-based analyses of high- and low-temperature fluids at the ESR. We also provide a description of the mineralogy of the uppermost section of conjugate high-temperature chimney material. Our data reveal that there are significant differences in the chemical composition of the fluids between the two ridge segments, even though the composition of the host basalt is similar, so the effects of additional processes, such as phase separation, on fluid chemistry, are interrogated. We also show that patterns of mineral zonation in the vent chimneys are generally similar to those observed at sediment-starved mid-ocean ridge hydrothermal sites, although chimneys that currently vent fluids with lowest Cl are more anhydrite-rich. Finally, we compare our results with existing data for other hydrothermal systems in back-arc basin and mid-ocean ridge (MOR) settings.

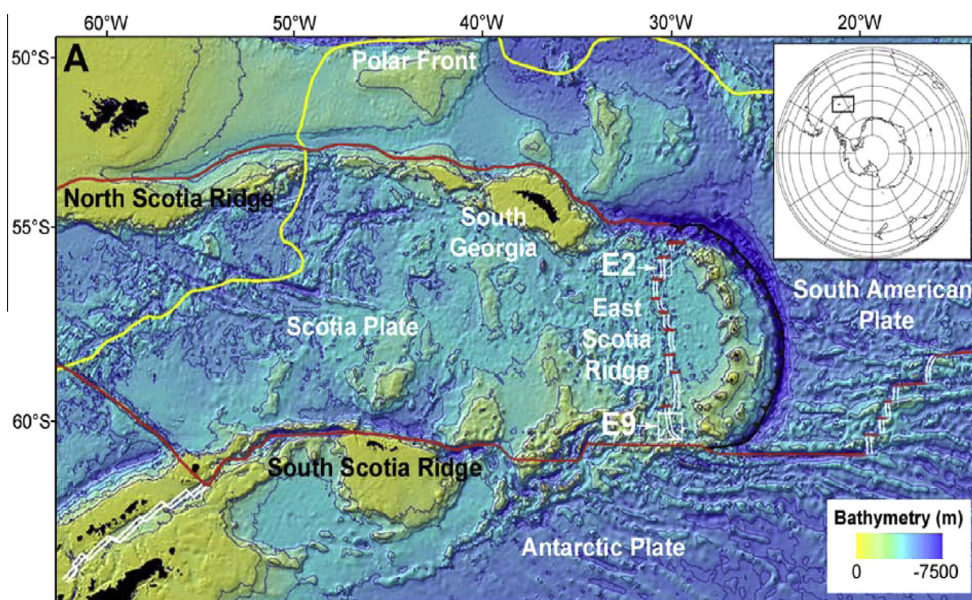


Fig. 1. Location of the E2 and E9 hydrothermal vent fields on the ESR back arc basin, South Atlantic Ocean. After [Marsh et al. \(2012\)](#).

2. GEOLOGIC SETTING

The ESR is an active back-arc spreading centre located to the west of the South Sandwich island arc in the South Atlantic Ocean (Fig. 1). It is currently extending at a full spreading-rate of 62–70 mm/yr (Livermore et al., 1997; Larter et al., 2003), separating the Scotia Plate to the west from the much smaller Sandwich Plate, which extends no more than ~300 km to the east. Although spreading was initiated more than 15 Myr ago, spreading in the south of the ridge commenced much more recently (probably less than 3 Myr ago) (Bruguier and Livermore, 2001). The spreading centre consists of ten segments, from E1 in the north, to E10 in the south (Livermore et al., 1997). The ridge is rift-like in the central part of the back-arc, with faulted median valleys similar to those observed on the Mid-Atlantic Ridge, and lavas are typically dominated by mid-ocean ridge basalt (MORB)-like compositions (Fretzdorff et al., 2002; Leat et al., 2004). In contrast, segments E2 and E9, near the northern and southern ends of the back-arc, respectively, both display axial volcanic ridges (AVRs), thought to be in response to inflow of mantle into the back-arc around the north and south edges of the slab (Livermore et al., 1997; Leat et al., 2000; Bruguier and Livermore, 2001). Lavas mainly range from basalt to basaltic andesite and are primarily low-K tholeiites, although some samples show medium-K compositions (Fig. 2; Fretzdorff et al., 2002; Leat et al., 2000, 2004). The mantle sampled in segments E2 and E9 differs from the mantle sampled in central ridge segments by having higher ratios of Nb, Ba and Th relative to Yb, and generally lower $^{143}\text{Nd}/^{144}\text{Nd}$ and higher $^{87}\text{Sr}/^{86}\text{Sr}$ ratios, which are indicative of E-type, rather than N-type MORB (Leat et al., 2004).

These segments also carry a subduction component, indicated most obviously by their enrichment in lead relative to MORB (Fretzdorff et al., 2002; Leat et al., 2004). The tectonic setting of segments E2 and E9, close to the edge of the subducting slab, is a probable setting for the Troodos Massif in Cyprus (Pearce and Robinson, 2010). This is arguably the world's most complete and best-studied ophiolite complex, and it is also host to economically valuable sulphide ore deposits (Bear, 1963).

The presence of an axial magma chamber reflector underlying the AVR on segment E2 (Livermore et al., 1997), and evidence for the presence of small pockets of magma remaining from a recent (<0.1 Myr ago) eruption event beneath the AVR on segment E9 (Bruguier and Livermore, 2001), have made these segments the target of investigations for hydrothermal activity (German et al., 2000).

2.1. The E2 hydrothermal vent field

The E2 vent field is located just south of the AVR, between $56^{\circ}5.2'$ and $56^{\circ}5.4'S$ and between $30^{\circ}19'$ and $30^{\circ}19.35'W$ at ~2600 m water depth (Fig. 3a and b). Steep-sided fissures run north–south through the centre of the site, between $30^{\circ}19.10'$ and $30^{\circ}19.15'W$, which is filled with pillow basalts. Extinct and actively venting chimneys are clustered along the fissures. 'Dog's Head' consists of a complex of four chimneys, up to ~12 m high, that actively vent black smoker fluids at temperatures of up to 351 °C (Fig. 4a). The 'Sepia' vent site lies 75 m to the south east of Dog's Head. Fluids issue from the top and the underside (flange) of a bulbous 'mushroom'-shape structure that is ~11 m high (Fig. 4b). The fluids sampled from the flange

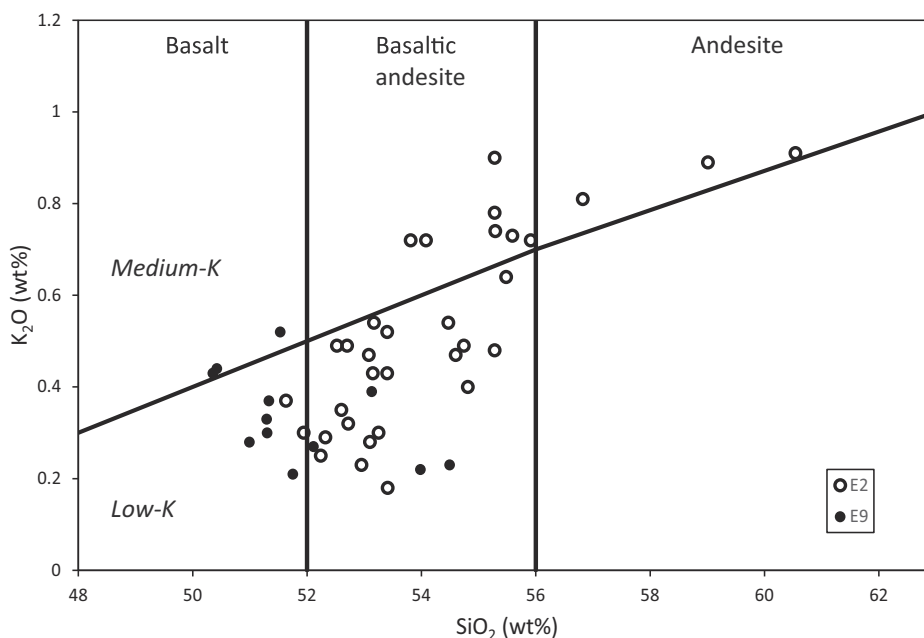


Fig. 2. K_2O vs. SiO_2 for volcanic glasses from segments E2 and E9 of the East Scotia Ridge. Data are from Leat et al. (2000), Fretzdorff et al. (2002) and Leat et al. (2004). Series boundaries and nomenclature from Peccerillo and Taylor (1976).

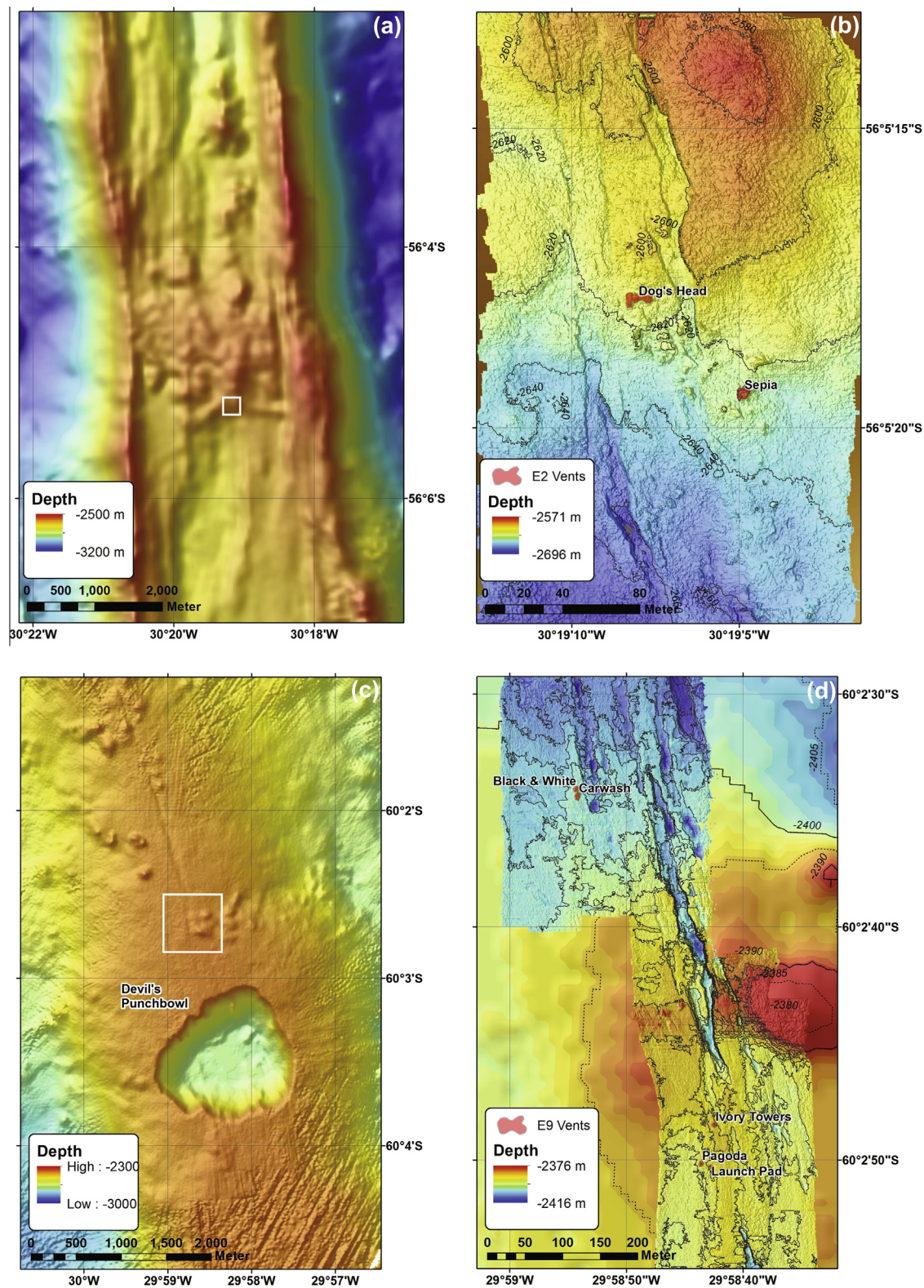


Fig. 3. (a) Ship-based swath bathymetry of the E2 segment of the ESR. Area outlined in white shows the area of the high-resolution map (b). (b) Ship- and ROV-based bathymetry showing the location of high-temperature vents in the E2 hydrothermal field. (c) Ship-based swath bathymetry of the E9 segment of the ESR. Area outlined in white shows the area of the high-resolution map (d). The major collapse caldera, Devil's Punchbowl, is clearly visible. (d) Ship- and ROV-based swath bathymetry showing the position of active vents in the E9 hydrothermal field. High resolution bathymetric contours are at 1 m intervals.

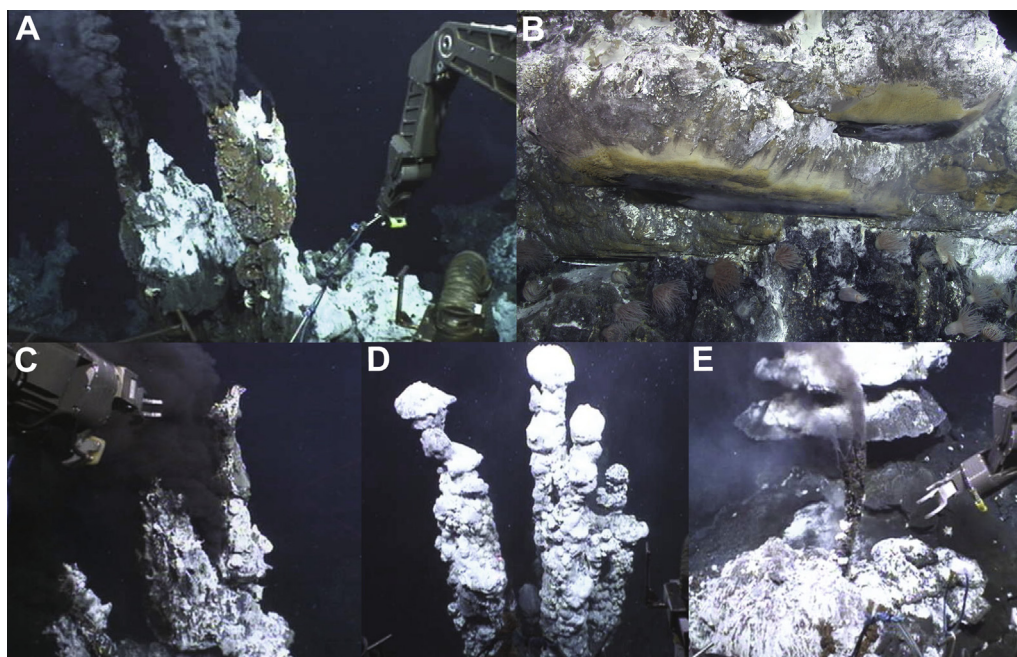


Fig. 4. Images showing: (A) Dog's Head chimney; (B) Sepia flange structure; (C) Black & White chimney; (D) Ivory Tower chimney and (E) Pagoda chimney.

are slightly cooler (313 °C) than the fluids sampled from the top of the structure (up to 353 °C). Numerous areas of diffuse flow were also observed around the vent field, with temperatures varying from 3.5 to 20 °C, compared with a background temperature of ~ 0.005 °C.

2.2. The E9 hydrothermal vent field

The E9 vent field is located north of a major collapse caldera ('Devil's Punchbowl') on the axial volcanic ridge of the E9 ridge segment, at ~ 2400 m water depth (Fig. 3c and d). Two areas of high temperature hydrothermal activity were discovered, between $60^{\circ}02.57'$ and $60^{\circ}02.84'S$ and between $29^{\circ}58.71'$ and $29^{\circ}58.90'W$. The distribution of these active fields, as well as inactive chimneys, appears to be associated with fissures parallel to the ridge axis, aligned NNW from the edge of the caldera across an otherwise relatively flat and unvaried terrain of sheet lavas (Fig. 3c; Rogers et al., 2012).

Two chimney structures occur in close proximity in the northern part of the E9 vent field. 'Black & White' is ~ 10 m high with multiple vents issuing high temperature fluids (up to 383 °C) at its summit (Fig. 4c). Lower down the chimney, wispy smoke can be seen issuing from beneath flange-type structures. The base of the chimney is surrounded by sulphide rubble that is probably indicative of chimney collapse in the past. A second chimney, 'Carwash', is located < 5 m south of Black & White. This chimney is ~ 10 m high and is currently venting only low temperature fluids. Between the two chimneys, lower temperature diffuse flow (5–19 °C) issues from small sulphide structures and cracks in the sheet lavas (Marsh et al., 2012). The background temperature at E9 ranged from -1.3 to -0.11 °C (Rogers et al., 2012).

The southern area of the vent field is characterised by active and extinct chimneys and diffuse flow fields distributed parallel to the ridge axis. High temperature fluids (348–351 °C) issue from three chimney structures. 'Ivory Towers' is located to the north of the vent field, ~ 30 m south of an area of low temperature diffuse flow, and is formed of two chimney complexes on a sulphide platform. One of these chimney complexes is ~ 7 m in height and issues high temperature (348 °C) fluids through a number of exits, including clusters of 'beehive' diffusers (Fig. 4d). The other complex consists of 5 individual chimneys with bulbous tops that do not visibly emit high-temperature fluid. Extensive wispy smoke is nevertheless observed from flange structures located close to the base of the chimney.

Approximately 50 m to the south of Ivory Towers two further structures occur in close proximity. At 'Pagoda', buoyant high-temperature fluid pools beneath a series of flanges (Fig. 4e). Similar flange-trapped fluid pools occur at 'Launch Pad' ~ 10 m to the west, where there is also a single black smoker chimney (Marsh et al., 2012). The southernmost limit of the vent field is marked by several inactive chimney structures, which lie ~ 100 m south of Pagoda.

3. METHODS

3.1. Collection of high- and low-temperature vent fluids, and chimney material

High temperature vent fluids were collected in 750-mL titanium (Ti) syringe samplers (Edmond et al., 1992), equipped with an Inductively Coupled Link (ICL) high-temperature sensor. For optimal sampling of focused flow, the chimney orifice was usually widened by breaking off the

tip with the arm of the ROV. The nozzle of the sampler was then inserted into the orifice, and the fluid was allowed to enter the bottle once a steady temperature reading was obtained. In the case of diffuse flow, the Ti samplers were used in conjunction with a specially-constructed Ti diffuse sampler, which was used to prevent entrainment of surrounding seawater into the path of the fluid during sampling. Where possible, fluid samples were taken towards the end of the ROV dive, to minimize the loss of gases and precipitation of minerals.

After sampling of high-temperature vent fluids, the uppermost section of the chimney structure (usually ~20 cm in length) through which the fluid was flowing was removed using the ROV manipulator arm and transferred to the ROV basket. Back on board the ship, the chimney samples were photographed and their dimensions noted. After drying in air, the sample was wrapped in bubble wrap and stored at ambient temperature.

3.2. Chemical analysis of vent fluids

As soon as the Ti-samplers returned to the surface, they were rinsed in Milli-Q water and the fluid was withdrawn. Separate sub-samples were collected for (i) refractive index, (ii) alkalinity, (iii) pH, (iv) gases, including H₂S, (v) anions and silica and (vi) O and H isotopes, in that order. The remainder of the sample (the 'bulk') was emptied into an acid-cleaned 1-L HDPE bottle for analysis of all other constituents, including cations and the transition metals. This sample was acidified (1%) with thermally distilled (TD) HNO₃. Any solid material ('dregs') that had presumably precipitated as the sample cooled was washed into an acid-cleaned 30 mL HDPE bottle with Milli-Q water and acidified (1%) with TD HNO₃.

Onboard the ship, alkalinity was determined by potentiometric Gran titration with 0.05 M HCl, using IAPSO seawater as a standard. The estimated 1 σ precision of this technique is $\pm 1.3\%$. pH was determined by ion specific electrode (± 0.05 units), and H₂S was determined by iodimetric titration with 0.1 M Na₂S₂O₃ ($\pm 2\%$). Anions (Cl⁻, Br⁻ and SO₄²⁻) were measured by ion chromatography (IC; Dionex ICS2500). Repeat analysis of IAPSO seawater as well as single anion standards indicates that the precision of Cl⁻ and SO₄²⁻ analyses is $< \pm 1\%$; for Br⁻ it is better than $\pm 2\%$.

Back onshore, the bulk sample was filtered through a 0.2 μ m polycarbonate filter. Particulate material retained on the filters was dissolved in 10 mL of 50% TD HNO₃ at 60 °C for several days, and then transferred to a Teflon microwave digestion vessel and microwaved at 400 W for 3 min. This step was repeated as necessary until the filter had completely dissolved. The digested sample was then transferred to a 15 mL Savillex vial with Milli-Q water and evaporated to dryness. 10 mL of 1.6 M TD HNO₃ was added to the vial, the sample was evaporated to dryness, and this step was repeated. Finally, the sample was dissolved in 10 mL of 1.6 M HNO₃ and its mass was determined. The 'dregs' sample was filtered, dissolved, dried down and re-dissolved in the same way. The concentration of cations was determined in each fraction (see

below), and the overall composition of the vent fluids was reconstructed.

All onshore analyses (except $\delta^{18}\text{O}$ and δD) were conducted at the National Oceanography Centre in Southampton. Concentrations of Li, Na, K, Ca, Mn and Sr in each fraction were determined by inductively coupled plasma optical emission spectroscopy (ICP-OES; Perkin Elmer Optima 4300DV). Concentrations of B, Fe, Cu, Zn, Cs and Ba were determined by ICP mass spectrometry (ICP-MS; Perkin Elmer DRC II). The accuracy and precision of both ICP-OES and ICP-MS measurements was determined by repeat analysis of a seawater standard (CRM seawater from High Purity Standards™). Precision was better than 2% for all elements, and the measured concentrations of all elements except the transition metals (which have very low concentrations in CRM seawater relative to the vent fluids) were within 2% of the certified values. Silica was determined by colourimetry using the silicomolybdate method (Strickland and Parsons, 1968), and fluoride was determined by IC equipped with a sample loop of 250 μ L (vs. 10 μ L for the other anions). The precision of these analyses was better than $\pm 5\%$. The Sr isotopic composition of the bulk fluid sample was determined by thermal ionisation mass spectrometry (VG Sector 54). Briefly, Sr was separated from the sample matrix by cation exchange chromatography on Sr-spec resin (Eichrom). The purified sample was loaded using a Ta activator solution onto single Ta filaments, and the ⁸⁷Sr/⁸⁶Sr ratio of the sample was determined. Analyses of the NIST987 Sr isotope standard, made during the course of this work, give ⁸⁷Sr/⁸⁶Sr = 0.710245 ± 0.000020 (2σ , $n = 3$), which is within error of the certified value (0.710250).

Oxygen and hydrogen isotope analysis of vent fluid samples was carried out by cavity ring-down spectroscopy (CDRS) at Picarro Inc. (Sunnyvale, California). Briefly, 2 μ L of sample was vaporized in a Picarro A0211 high precision vaporizer, and allowed to equilibrate with ultra-high purity dry nitrogen gas before introduction into a Picarro L115-i water vapour analyser for isotope analysis (Powell et al., 2011). Each sample was analysed by 10 sequential injections, and results are based on the last 8 injections to minimize potential memory effects. All data were run through the *ChemCorrect*™ software developed by Picarro Inc. to remove any contamination from organic components. Isotope ratios were normalised to the VSMOW seawater reference material. Replicate analyses of individual samples indicate that the reproducibility of the analyses is $\sim 0.1\%$ for $\delta^{18}\text{O}$ and $\sim 0.3\%$ for δD .

3.3. Petrologic analysis of chimney material

Back in the laboratory, the chimney samples were described, re-photographed and then cut for thin sectioning. Sections were designed to investigate mineral zonation and textures observed within the chimney walls. The cut surfaces were also described and photographed. Polished blocks were made to investigate sulphide mineralisation and polished thin sections were made to investigate the gangue mineralogy. Thin sections were analysed under both

transmitted and reflected light, and recorded by photomicrograph. Polished blocks were analysed by reflected light microscopy only. Finally, any loose material from the inner and outer chimney wall was scraped off, ground and analysed by X-ray diffraction (XRD) spectroscopy to characterise sulphate and sulphide phases.

4. RESULTS

4.1. Composition of vent fluids

We collected 11 high-temperature and 6 low-temperature water samples from two different vent sites on the E2 segment, and 12 high-temperature and 8 low-temperature water samples from 4 different vent sites on the E9 segment (Table 1). Of the high-temperature samples, all but 4 contained <5 mmol/kg Mg and thus consist of <10% bottom seawater. The zero-Mg end-member concentrations for each vent are calculated, as is the usual practise, by extrapolating from the composition of bottom seawater collected at each vent field, through the Mg concentration measured in the samples from a given vent (Fig. 5). End-member concentrations are given in Table 2.

4.1.1. Temperature

The low-Mg vent fluids sampled at both sites on E2 have temperatures of 351 and 353 °C, although the temperature of the fluid seeping through the flange around the hydrothermal chimney at Sepia was slightly lower (313 °C). Diffuse fluids when extrapolated to zero Mg yield temperatures slightly lower (311 °C) than the high-temperature fluids, suggesting that they have cooled during mixing with bottom seawater in the sub-surface prior to emission at the seafloor. Vent fluids sampled from chimneys to the south of the E9 vent field also have temperatures close to ~350 °C, but the Black & White vent to the north of the vent field is significantly hotter, at 383 °C. Diffuse fluids at this site extrapolate to slightly lower temperatures (333 °C), whereas diffuse fluids from the southern vent sites extrapolate to temperatures somewhat higher (363–382 °C) than those measured in the high-temperature fluids.

4.1.2. Mg and SO₄

With the exception of Black & White, Mg and SO₄ decrease linearly from their concentrations in seawater to nearly zero. Low Mg fluids from Black & White tend to have higher SO₄, and the end-member (zero Mg) fluid is predicted to contain 3.6 mM of SO₄. This could be due either to dissolution of anhydrite by circulation of cooler fluids in the subsurface prior to venting, or to dissolution within the samplers of chimney particles that may have been entrained during sampling.

4.1.3. pH, alkalinity, H₂S and Si

Lowest recorded pH values for high-temperature vent fluids are ~3.0 at segment E2 but, with the exception of Ivory Tower (3.08), they are slightly higher at E9 (~3.3). The alkalinity of the vent fluids is negative at all of the vent sites, due to mineral acidity. The H₂S content of the vent

fluids at E2 is ~7 mM, whereas concentrations at E9 are slightly higher, reaching ~9.5 mM at Black & White, and up to ~14 mM at the southern vent sites (Fig. 5a). Si concentrations range from 17.7 to 22.6 mM at E2, and are slightly lower at the southern vents sites at E9 (12.7–14 mM). The Si concentration of end-member fluids from Black & White is lower again, at 8.2 mM.

4.1.4. Cl, Br and F

While end-member Cl concentrations (532–536 mM) are close to local bottom seawater (540 mM) at E2, all of the E9 fluids have much lower levels of Cl than seawater (Fig. 5b). The Black & White vents have concentrations as low as 98 mM, whereas concentrations at the southern E9 sites are slightly higher (179–220 mM). End-member Br concentrations show similar patterns, although ratios of Br/Cl are slightly higher than bottom seawater (1.54×10^{-3}), ranging from 1.57×10^{-3} at Dog's Head to 1.75×10^{-3} at Black & White. All of the vent fluids have lower F concentrations ([F]) than seawater (62.8 μM). Fluids from E2 and Black & White and Ivory Tower have similar [F], between 34.6 and 40.1 μM, whereas the F content of end-member fluids from Pagoda and Launch Pad are slightly higher (respectively, 54.4 and 53.7 μM).

4.1.5. Alkali and alkaline earth elements, and B

Concentrations of the alkali elements (Na (Fig. 5c), Li (Fig. 5d), K and Cs) co-vary with Cl, because of charge balance constraints. To eliminate this effect, alkali element concentrations can be normalised to Cl (Table 3). Vent fluids from E2 have lower molar Na/Cl ratios than seawater (0.86), ranging from 0.79 to 0.80, whereas fluids from the southern E9 vent field have Na/Cl ratios slightly higher than seawater, 0.87–0.91. The Na/Cl ratio of Black & White end-member fluids (0.98) is distinctly higher than seawater. To our knowledge, this is the highest Na/Cl ratio ever measured in a seafloor hot spring. Both absolute and Cl-normalized end-member Li and Cs concentrations are much higher than seawater at all vent sites. End-member K/Cl ratios are also higher than seawater, but the concentration of K in Black & White fluids is lower than it is in bottom seawater.

Concentrations of the alkaline earth elements (Ca (Fig. 5e), Sr and Ba) also co-vary with Cl, but less closely compared to the alkalis. The relationship between these elements and Cl at Black & White is especially scattered, presumably because of dissolution/precipitation of anhydrite and barite. On average ~50% of vent fluid Ba was recovered from solid material that had precipitated in the Ti samplers during retrieval. End-member Ba is higher than seawater, as are end-member Sr and Ca concentrations at E2 sites, whereas end-member Sr and Ca concentrations are lower than seawater at E9. End-member Ca/Cl ratios are all greater than seawater, whereas Sr/Cl is lower than seawater at the southern E9 sites and higher than seawater at E2 (Table 3). End-member Sr/Cl is much higher than seawater at Black & White, presumably because of dissolution of anhydrite.

All of the vent fluids are slightly enriched in boron relative to seawater. End-member molar B/Cl ratios are

Table 1

Measured concentrations of chemical species in high- and low-temperature hydrothermal fluids from the East Scotia Ridge.

| Location/Type | Sample # | <i>T</i> °C | Mg mmol/ kg | pH | Alk mEq/ L | Na mmol/ kg | K mmol/ kg | Li μmol/ kg | Cs nmol/ kg | Ca mmol/ kg | Sr μmol/ kg | Ba μmol/ kg | SO ₄ mM | Cl mM | Br μM | F μM | Si mM | H ₂ S mM | Mn μmol/ kg | Fe μmol/ kg | Cu μmol/ kg | Zn μmol/ kg | B μmol/ kg | δ ¹⁸ O | δD | ⁸⁷ Sr/ ⁸⁶ Sr | |
|-----------------------|----------------|----------------|-------------------|------|------------------|-------------------|------------------|-------------------|-------------------|-------------------|-------------------|-------------------|-----------------------|----------|----------|---------|----------|------------------------|-------------------|-------------------|-------------------|-------------------|------------------|-------------------|------|------------------------------------|--|
| <i>E2</i> | | | | | | | | | | | | | | | | | | | | | | | | | | | |
| Dog's Head Chimney | JC42-130-B2-05 | 323 | 2.11 | 3.02 | −0.86 | 429 | 38.0 | 579 | 579 | 29.9 | 102 | 18.3 | 2.3 | 542 | 844 | 37.7 | 17.1 | 6.2 | 1960 | 1170 | 11.2 | 27.4 | 531 | 1.0 | 1.3 | 0.704352 | |
| Dog's Head Chimney | JC42-130-B2-08 | 323 | 2.28 | 3.03 | −0.83 | 431 | 38.0 | 571 | 574 | 30.1 | 99.7 | 6.00 | 2.5 | 540 | 843 | 39.1 | 13.8 | 6.2 | 1960 | 1180 | 19.0 | 151 | 520 | 0.9 | 1.1 | 0.704355 | |
| Dog's Head Chimney | JC42-132-Y1-07 | 351 | 1.02 | 3.05 | −0.74 | 427 | 38.8 | 598 | 594 | 30.0 | 103 | 23.0 | 3.7 | 528 | 837 | 42.8 | 17.2 | 6.9 | 2020 | 1350 | 1.56 | 11.8 | 533 | 1.2 | 1.8 | 0.704241 | |
| Sepia Chimney | JC42-130-Y2-01 | 351 | 12.1 | 3.66 | −0.10 | 429 | 31.8 | 469 | 458 | 26.7 | 98.0 | 11.9 | 7.4 | 534 | 800 | 39.0 | 13.9 | 5.3 | 1600 | 815 | 14.8 | 150 | 520 | 0.8 | 1.5 | nd | |
| Sepia Chimney | JC42-130-Y2-04 | 351 | 2.34 | 3.14 | −0.66 | 420 | 37.1 | 571 | 567 | 30.6 | 101 | 17.0 | 2.2 | 535 | 834 | 41.7 | nd | 6.7 | 1990 | 993 | 18.3 | 160 | 528 | 0.9 | 1.3 | nd | |
| Sepia Chimney | JC42-135-Y2-01 | 353 | 1.94 | 3.10 | −0.62 | 421 | 37.1 | 591 | 578 | 30.9 | 101 | 13.8 | 2.1 | 531 | 848 | 39.6 | 21.3 | 6.8 | 1980 | 959 | 1.81 | 24.3 | 540 | 0.9 | 1.4 | nd | |
| Sepia Chimney | JC42-135-Y2-04 | 353 | 1.99 | 3.11 | −0.69 | 423 | 37.1 | 587 | 576 | 31.0 | 102 | 14.8 | 1.9 | 528 | 848 | 38.8 | 21.2 | 6.8 | 1980 | 976 | 18.6 | 134 | 523 | 0.9 | −0.2 | nd | |
| Sepia Chimney | JC42-135-B2-05 | 347 | 1.60 | 3.05 | −0.72 | 418 | 37.0 | 591 | 586 | 31.1 | 101 | 22.8 | 1.9 | 535 | 852 | 43.1 | 21.5 | 7.0 | 1970 | 971 | 13.8 | 133 | 559 | 1.4 | 1.4 | 0.704167 | |
| Sepia Chimney | JC42-135-B2-08 | 347 | 1.61 | 3.07 | −0.74 | 419 | 37.3 | 591 | 580 | 30.9 | 102 | 18.6 | 1.8 | 532 | 833 | 36.7 | 21.4 | 7.0 | 1990 | 960 | 5.46 | 26.7 | 535 | 1.0 | −0.5 | 0.704171 | |
| Sepia Flange | JC42-132-B1-02 | 313 | 4.04 | 2.93 | −0.99 | 413 | 34.9 | 542 | 548 | 28.2 | 93.4 | 19.4 | 3.6 | 521 | 837 | 40.2 | 4.06 | 6.5 | 2040 | 728 | 0.61 | 130 | 540 | 0.9 | −0.6 | nd | |
| Sepia Flange | JC42-132-B1-03 | 313 | 4.21 | 2.9 | −1.07 | 414 | 35.0 | 547 | 550 | 28.1 | 92.9 | 15.4 | 2.6 | 516 | 803 | 42.9 | 16.7 | 6.4 | 2050 | 737 | 1.87 | 150 | 552 | 0.9 | −0.8 | nd | |
| Diffuse Flow | JC42-133-B2-05 | 20 | 49.9 | 6.39 | 2.38 | 458 | 11.0 | 52.1 | 26.5 | 11.0 | 87.4 | 2.12 | 26.5 | 541 | 830 | 58.1 | 1.24 | 0.1 | 92.9 | 4.13 | 0.03 | 0.12 | 441 | 0.0 | 0.0 | nd | |
| Diffuse Flow | JC42-133-B2-08 | 20 | 50.1 | 6.39 | 2.23 | 459 | 10.9 | 52.5 | 26.3 | 11.0 | 87.8 | 2.15 | 26.5 | 540 | 835 | 59.5 | 1.26 | 0.1 | 94.2 | 3.95 | 0.09 | 0.39 | 432 | 0.0 | 0.5 | nd | |
| Diffuse Flow | JC42-133-Y2-01 | 3.5 | 52.6 | 7.56 | 2.60 | 464 | 10.0 | 28.9 | 3.99 | 10.2 | 88.1 | 0.46 | 27.8 | 542 | 831 | 63.6 | 0.23 | bdl | 9.94 | 2.55 | 0.13 | 0.22 | 421 | −0.2 | −0.5 | nd | |
| Diffuse Flow | JC42-133-Y2-04 | 3.5 | 52.7 | 7.59 | 2.46 | 464 | 9.95 | 28.7 | 3.51 | 10.2 | 88.1 | 0.41 | 27.2 | 531 | 817 | 63.6 | 0.23 | bdl | 9.76 | 2.17 | 0.10 | 0.54 | 424 | 0.0 | −0.1 | nd | |
| Diffuse Flow | JC42-134-B1-02 | 8.1 | 51.7 | 6.84 | 2.34 | 463 | 10.4 | 37.4 | 11.8 | 10.4 | 88.0 | 2.07 | 27.2 | 535 | 821 | 59.6 | 0.51 | bdl | 40.1 | 6.63 | 0.07 | 0.87 | 420 | 0.0 | 0.2 | nd | |
| Diffuse Flow | JC42-134-B1-03 | 8.1 | 51.8 | 6.85 | 2.31 | 464 | 10.4 | 36.9 | 12.1 | 10.5 | 88.3 | 2.36 | 27.3 | 540 | 819 | 65.4 | 0.51 | bdl | 40.3 | 6.75 | 0.10 | 1.29 | 418 | 0.0 | 0.7 | nd | |
| <i>E9</i> | | | | | | | | | | | | | | | | | | | | | | | | | | | |
| Black & White Chimney | JC42-140-Y2-01 | 380 | 8.02 | 3.42 | −0.31 | 152 | 4.69 | 109 | 54.7 | 4.69 | 21.9 | 3.22 | 5.0 | 163 | 262 | 40.2 | 1.09 | 7.8 | 169 | 428 | 10.5 | 58.7 | 450 | 0.7 | 1.3 | 0.707598 | |
| Black & White Chimney | JC42-140-Y2-04 | 380 | 0.58 | 3.52 | −0.19 | 99.1 | 5.53 | 114 | 63.6 | 5.53 | 16.4 | 4.14 | 2.2 | 106 | 199 | nd | 7.98 | 8.2 | 197 | 803 | 26.1 | 20.3 | 446 | 0.6 | 0.4 | 0.706029 | |
| Black & White Chimney | JC42-142-Y2-01 | 383 | 8.35 | 3.81 | 0.03 | 156 | 11.6 | 113 | 54.2 | 11.6 | 50.4 | 4.14 | 11.2 | 166 | 271 | 39.8 | 7.05 | 8.1 | 169 | 644 | 27.0 | 5.07 | 447 | 0.3 | 0.5 | nd | |

| | | | | | | | | | | | | | | | | | | | | | | | | | | |
|-----------------------|----------------|-----|------|------|-------|-----|------|------|------|------|------|------|------|-----|-----|------|------|------|------|------|------|------|-----|------|------|----------|
| Black & White Chimney | JC42-142-Y2-04 | 383 | 2.37 | 3.44 | -0.33 | 111 | 6.10 | 113 | 61.5 | 6.10 | 22.7 | 3.21 | 4.6 | 124 | 212 | 40.9 | 7.90 | 8.9 | 189 | 649 | 38.1 | 8.56 | 463 | 0.4 | 0.6 | nd |
| Black & White Chimney | JC42-145-Y1-06 | 357 | 15.8 | 3.73 | -0.08 | 205 | 7.83 | 102 | 45.0 | 7.83 | 44.5 | 1.74 | 11.1 | 227 | 352 | 39.4 | 5.82 | 8.2 | 139 | 803 | 161 | 25.0 | 458 | 0.3 | 0.4 | nd |
| Black & White Chimney | JC42-145-Y1-07 | 357 | 14.4 | 3.77 | -0.09 | 195 | 7.77 | 102 | 47.6 | 7.77 | 43.1 | 1.71 | 10.7 | 214 | 338 | 36.2 | 5.99 | 7.9 | 144 | 592 | 55.3 | 20.8 | 458 | 0.3 | 0.4 | nd |
| Carwash Diffuse Flow | JC42-140-B2-05 | 11 | 52.0 | 5.96 | 2.21 | 458 | 9.83 | 31.6 | 2.11 | 9.94 | 85.4 | 0.33 | 27.6 | 539 | 844 | 64.0 | 0.32 | 0.1 | 4.18 | 5.57 | 0.07 | 0.48 | 418 | 0.3 | -0.1 | nd |
| Carwash Diffuse Flow | JC42-140-B2-08 | 11 | 51.5 | 5.95 | 2.22 | 452 | 9.70 | 32.0 | 2.14 | 9.83 | 84.3 | 0.33 | 27.2 | 530 | 814 | 63.6 | 0.31 | 0.2 | 4.04 | 5.33 | 0.12 | 0.16 | 423 | 0.0 | -0.6 | nd |
| N Field Diffuse Flow | JC42-145-Y2-01 | nd | 48.0 | 5.22 | 2.24 | 427 | 9.28 | 40.5 | 3.45 | 9.28 | 78.3 | 0.97 | 24.8 | 486 | 726 | 57.3 | 1.46 | 1.7 | 2.99 | 8.47 | 0.10 | 0.31 | 435 | -0.1 | -0.3 | nd |
| N Field Diffuse Flow | JC42-145-Y2-04 | nd | 48.0 | 5.22 | 2.24 | 428 | 9.32 | 33.8 | 3.76 | 9.32 | 79.6 | 1.06 | 25.7 | 505 | 752 | 57.1 | 1.42 | 1.2 | 3.07 | 11.2 | 0.14 | 0.86 | 440 | 0.0 | -0.5 | nd |
| Ivory Tower Chimney | JC42-142-B2-05 | 348 | 1.96 | 3.08 | -0.83 | 201 | 14.7 | 210 | 160 | 5.79 | 26.7 | 6.14 | 0.8 | 227 | 375 | 42.3 | 12.4 | 10.8 | 590 | 1070 | 13.9 | 23.9 | 458 | 0.7 | 1.3 | 0.705152 |
| Ivory Tower Chimney | JC42-142-B2-08 | 348 | 3.22 | 3.17 | -0.68 | 207 | 14.6 | 207 | 157 | 6.05 | 28.7 | 7.87 | 2.4 | 240 | 382 | 40.2 | 11.8 | 10.9 | 575 | 1250 | 85.2 | 40.0 | 455 | nd | nd | 0.705471 |
| Pagoda Chimney | JC42-144-Y1-06 | 351 | 0.84 | 3.44 | -0.20 | 196 | 14.8 | 215 | 158 | 6.42 | 27.6 | 9.47 | 1.3 | 227 | 379 | 54.7 | 13.9 | 10.5 | 461 | 831 | 32.4 | 20.0 | 461 | 0.6 | 0.1 | 0.705121 |
| Pagoda Chimney | JC42-144-Y1-07 | 351 | 2.34 | 3.40 | -0.29 | 202 | 14.5 | 208 | 155 | 6.40 | 28.4 | 4.94 | 2.2 | 234 | 382 | 54.7 | 13.3 | 10.2 | 444 | 528 | 2.8 | 14.9 | 465 | 0.7 | 0.3 | 0.705456 |
| Launch Pad Chimney | JC42-144-B1-02 | 351 | 4.45 | 3.21 | -0.56 | 188 | 12.2 | 156 | 112 | 6.08 | 26.6 | 4.13 | 2.1 | 211 | 340 | 56.3 | 12.6 | 12.0 | 466 | 1110 | 557 | 40.6 | 467 | 0.5 | 0.2 | 0.706177 |
| Launch Pad Chimney | JC42-144-B1-03 | 351 | 12.9 | 3.57 | -0.13 | 237 | 11.8 | 138 | 94.0 | 6.72 | 36.8 | 1.84 | 6.1 | 264 | 420 | 53.8 | 10.5 | 10.8 | 384 | nd | nd | nd | 467 | 0.8 | -0.2 | 0.707408 |
| S Field Diffuse Flow | JC42-141-B1-02 | 5 | 52.8 | 7.30 | 2.47 | 461 | 9.85 | 36.5 | 0.52 | 10.0 | 86.1 | 0.16 | 27.5 | 535 | 827 | 63.1 | 0.16 | bdl | 0.98 | 0.0 | 1.3 | 1.2 | 435 | nd | nd | nd |
| S Field Diffuse Flow | JC42-141-B1-03 | 5 | 52.7 | 7.37 | 2.45 | 462 | 9.79 | 36.2 | 0.37 | 10.0 | 85.9 | 0.23 | 27.2 | 529 | 820 | 63.3 | 0.16 | bdl | 0.82 | 1.2 | 0.9 | 1.1 | 417 | nd | nd | nd |
| S Field Diffuse Flow | JC42-141-Y1-06 | 20 | 50.2 | 5.91 | 2.07 | 451 | 9.91 | 36.7 | 6.33 | 9.99 | 83.9 | 0.55 | 26.1 | 520 | 799 | 61.8 | 1.08 | 0.1 | 18.9 | 5.4 | 0.1 | 0.2 | 430 | nd | nd | nd |
| S Field Diffuse Flow | JC42-141-Y1-07 | 20 | 50.5 | 5.97 | 2.03 | 455 | 9.87 | 44.1 | 5.69 | 10.1 | 84.0 | 0.50 | 26.4 | 527 | 801 | nd | 1.00 | 0.1 | 16.8 | 5.2 | 0.1 | 0.3 | 428 | nd | nd | nd |

nd: not determined.

bdl: below detection limit.

slightly higher than seawater (0.8×10^{-3}) at E2 (1.0×10^{-3} – 1.1×10^{-3}), but much higher than seawater at E9 (2.1×10^{-3} – 4.7×10^{-3}).

4.1.6. Transition metals

The concentration of Mn in the end-member fluids co-varies with Cl, so levels are highest in E2 fluids (2050–2220 $\mu\text{mol/kg}$) and much lower in E9 fluids (199–612 $\mu\text{mol/kg}$) (Fig. 5f). Fluids with highest Cl also have higher Zn ($\sim 160 \mu\text{mol/kg}$ at E2 vs. 20–41 $\mu\text{mol/kg}$ at E9); $\sim 50\%$ of Zn in E9 fluids was recovered from solid material that had precipitated in the Ti samplers, mainly sulphides. (There is a positive relationship between Zn and S concentrations in solid phases.)

Concentrations of Fe in end-member fluids (Fig. 5g) show no variation with Cl. Fe/Cl ratios are higher in E9 fluids (3.8×10^{-3} – 8.1×10^{-3}) than in E2 fluids (1.5×10^{-3} – 2.4×10^{-3}), as is the molar Fe/Mn ratio (1.8–4.0 at E9 vs. 0.4–0.6 at E2). Very little Fe ($<3\%$) was recovered from solid material in E2 samples, whereas 30–50% was present in solid phases in E9 samples. Copper also shows no variation with Cl, and in fact fluids with highest Cu are those with lowest Cl. Up to 20% of Cu was recovered from the solid phase in E2 samples, whereas most ($\sim 90\%$) of the Cu in E9 samples was recovered from solids, primarily as sulphides.

4.1.7. Sr, O and H isotopes

End-member $^{87}\text{Sr}/^{86}\text{Sr}$ ratios for E2 fluids range from 0.704035 to 0.704168 and are lower than the E9 end-members (0.70489–0.70514). The calculated end-member for Black & White is slightly higher, at 0.705762, but this is partly an artefact of the low Mg/Sr ratio due to dissolution of anhydrite. Anhydrite dissolution does not fractionate Sr isotopes (Mills and Elderfield, 1995), and would decrease the fluid Mg/Sr ratio without changing the $^{87}\text{Sr}/^{86}\text{Sr}$ ratio. The $^{87}\text{Sr}/^{86}\text{Sr}$ ratio of all of the fluids is slightly higher than the values reported for East Scotia Ridge lavas: lavas from E2 have $^{87}\text{Sr}/^{86}\text{Sr}$ ratios between 0.702897 and 0.703444 ($n = 10$; Leat et al., 2000), and lavas from E9 have $^{87}\text{Sr}/^{86}\text{Sr}$ ratios between 0.702940 and 0.703102 ($n = 7$; Fretzdorff et al., 2002; Leat et al., 2004).

The oxygen isotope ratio of the end-member fluids is slightly lower in the E9 vents ($\delta^{18}\text{O} = 0.5\text{‰}$ to 0.8‰), than in the E2 vents ($\delta^{18}\text{O} = 1.0\text{‰}$ to 1.1‰). All vent fluids are slightly enriched in ^{18}O relative to bottom seawater (0‰) (Fig. 5h). The end-member hydrogen isotope ratios show a similar pattern: δD values are slightly lower at E9 (0.2 – 0.5‰) than they are at E2 ($\sim 1.1\text{‰}$), and all vent fluids (except those emanating from the flange) are slightly enriched in D relative to bottom seawater (-0.1‰). The δD composition of the Sepia flange fluids is slightly depleted in D ($\delta D = -0.8\text{‰}$) relative to seawater.

4.2. Mineralogy of the uppermost section of the hydrothermal chimneys

Photographs showing representative cut sections through the chimney structures are shown in Fig. 6. Fig. 7 shows a series of photomicrographs that provide

evidence for the patterns of mineral zonation that are described below, in turn, for each chimney sample.

The uppermost section of the chimney from Dog's Head on the E2 segment is characterised by an inner surface consisting predominantly of coarse-grained, granular chalcopyrite, with minor pyrite, that grades into a more massive texture away from the chimney orifice. The chalcopyrite becomes intergrown with bornite in the outer part of this layer and, locally, bornite appears to replace the chalcopyrite (Fig. 7a). Covellite sometimes replaces both primary and secondary (chalcopyrite-replacement) bornite, and is most commonly found within cracks and along grain boundaries (Fig. 7a). The massive chalcopyrite-rich layer then grades into a zone that is mainly composed of fine grained anhydrite, with minor pyrite, chalcopyrite and occasional fibrous goethite. This zone becomes abruptly coarser grained and porous ($\sim 10\%$ porosity) towards the outside of the chimney, grading into a barite-dominated layer which extends to the outer chimney wall (Fig. 7b). The anhydrite–barite transition is associated with an increase in porosity (up to 20–30%). Sphalerite and chalcopyrite occur as monomineralic or polyminerally intergrown crystalline aggregates, occasionally with rare pyrite, within both anhydrite- and barite-rich layers. However, sphalerite rarely makes up more than 2% of the mineral phases. The outer surface of the chimney consists mainly of sulphides (mainly sphalerite and pyrite), with some Fe-, Mn- and Cu-oxides, and patches of barite and anhydrite. Alpha radiation counts (determined using a Geiger counter) were up to 6 times higher than background values on the outer surface of the chimney, due to substitution of ^{226}Ra for Ba (determined by gamma spectrometry) within the barite lattice.

The tip of the chimney sampled at Ivory Towers on E9 is also zoned. The inner part of the chimney consists of coarse-grained chalcopyrite aggregates, with relatively high porosity. This layer grades into a zone composed of fine- to medium-grained chalcopyrite, commonly intergrown with sphalerite ($\sim 40\%$) and pyrite ($\sim 15\%$) (Fig. 7c). The pyrite concentration increases outwards, away from the chimney orifice. Barite is present as crystalline aggregates within this layer, most commonly in pyrite-rich areas, and is occasionally mixed with minor anhydrite. The outer surface of the chimney consists of sulphide minerals (marcasite, sphalerite, and pyrite), anhydrite and barite.

Like Ivory Towers, the inner part of the tip of the chimney taken from Pagoda on E9 consists of coarse-grained chalcopyrite. The chalcopyrite becomes more fine-grained towards the outer part of this layer and is intergrown with pyrite and sphalerite, mixed with anhydrite. In contrast to Ivory Towers, sphalerite is relatively rare ($<2\%$) and minor quantities of bornite are present locally. The bornite is extensively replaced by covellite, which occurs in high concentrations within localised masses, particularly towards the outside of the chimney structure (Fig. 7d). The outer surface of the chimney is covered with soft, fine-grained grey-black oxides, together with various sulphide minerals (marcasite, chalcopyrite, sphalerite, pyrite and covellite).

By contrast to the other sites in the southern part of E9, the proportion of anhydrite in the uppermost section of the Launch Pad chimney is far higher ($\sim 45\%$). The innermost

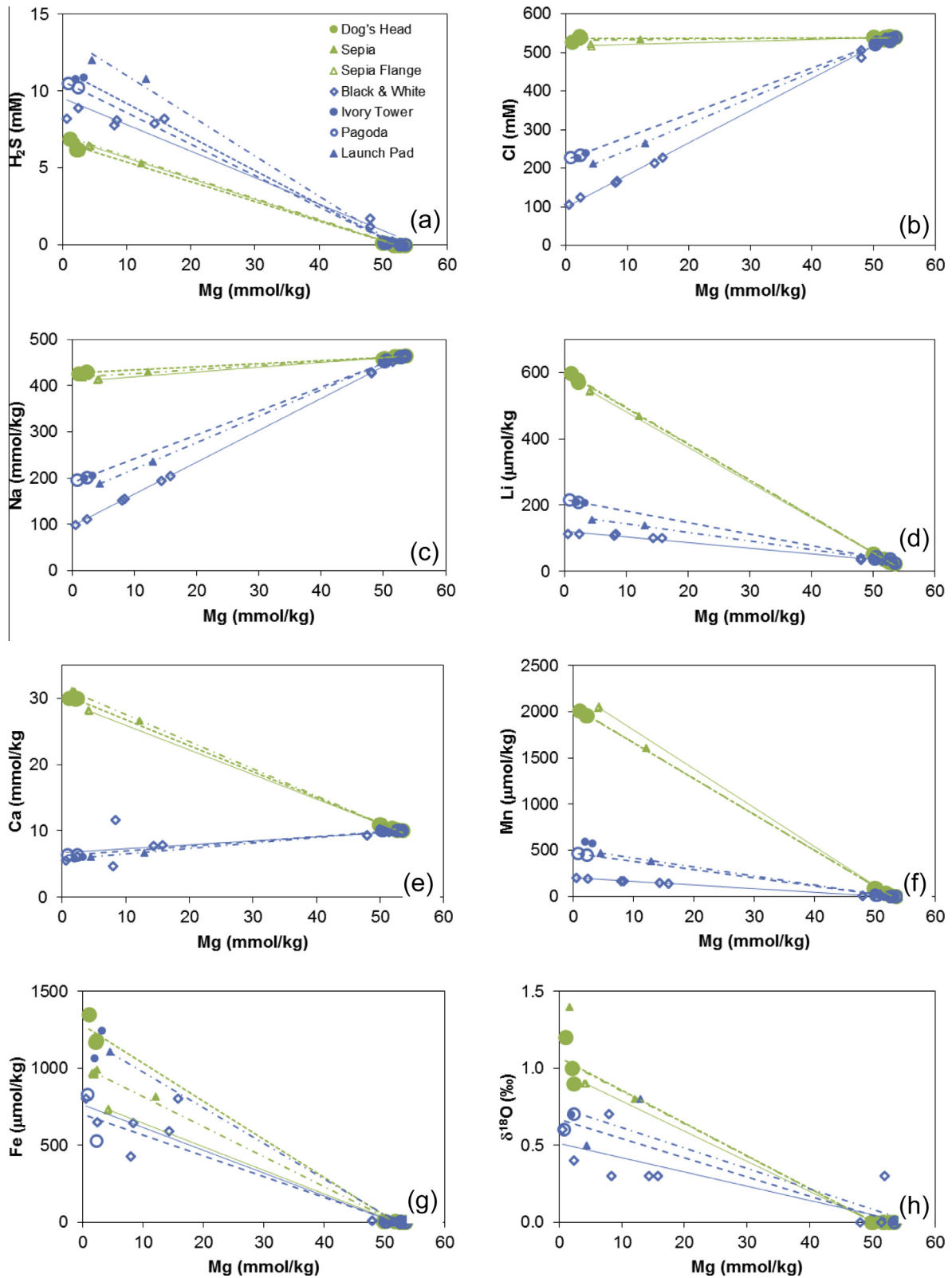


Fig. 5. Measured (a) H_2S , (b) Cl, (c) Na, (d) Li, (e) Ca, (f) Mn, (g) Fe and (h) $\delta^{18}\text{O}$ vs. Mg in high- and low-temperature vent fluids recovered from segments E2 (green; Dog's Head and Sepia) and E9 (blue; Black & White, Ivory Tower, Pagoda and Launch Pad) on the ESR. (For interpretation of the references to colour in this figure legend, the reader is referred to the web version of this article.)

Table 2
End-member composition of vent fluids from the East Scotia Ridge.

| Vent | Max T °C | Min Mg mmol/kg | pH* | Alk mEq/ L | Na mmol/ kg | K mmol/ kg | Li μ mol/ kg | Cs nmol/ kg | Ca mmol/ kg | Sr μ mol/ kg | Ba [†] μ mol/ kg | Cl mM | Br μ M | F μ M | Si mM | H ₂ S mM | Mn μ mol/ kg | Fe [†] μ mol/ kg | Cu [‡] μ mol/ kg | Zn [‡] μ mol/ kg | B μ mol/ kg | $\delta^{18}\text{O}$ | δD | ⁸⁷ Sr/ ⁸⁶ Sr |
|--------------------|------------|-------------------|------|------------------|-------------------|------------------|------------------------|-------------------|-------------------|------------------------|-------------------------------------|----------|---------------|--------------|----------|------------------------|------------------------|-------------------------------------|-------------------------------------|-------------------------------------|-----------------------|-----------------------|------------|------------------------------------|
| <i>E2</i> | | | | | | | | | | | | | | | | | | | | | | | | |
| Dog's Head | 351 | 1.02 | 3.02 | -0.92 | 428 | 39.3 | 602 | 603 | 30.7 | 102 | 23 | 536 | 842 | 39.1 | 17.7 | 6.7 | 2050 | 1280 | 19 | 150 | 532 | 1.1 | 1.5 | 0.704168 |
| Sepia | 353 | 1.60 | 3.05 | -0.80 | 419 | 38.1 | 606 | 598 | 31.7 | 102 | 18 | 532 | 838 | 38.4 | 22.6 | 7.1 | 2060 | 1010 | 19 | 160 | 542 | 1.1 | 1.4 | 0.704035 |
| Sepia Flange | 313 | 4.04 | 2.90 | -1.31 | 409 | 37.0 | 588 | 595 | 29.7 | 93.5 | 18 | 517 | 838 | 39.8 | 22.6 | 7.1 | 2220 | 794 | 1.9 | 160 | 556 | 1.0 | 0–0.8 | nd |
| <i>E9</i> | | | | | | | | | | | | | | | | | | | | | | | | |
| Black & White | 383 | 0.58 | 3.42 | -0.58 | 96 | 6.53 | 122 | 64.5 | 6.68 | 22.7 | 4.1 | 98.2 | 172 | 34.6 | 8.19 | 9.5 | 199 | 800 | 160 | 29 | 458 | 0.5 | 0.5 | 0.705762 |
| Ivory Tower | 348 | 1.96 | 3.08 | -0.92 | 191 | 14.8 | 217 | 164 | 6.01 | 25.4 | 9.5 | 220 | 361 | 40.1 | 12.7 | 11 | 612 | 1210 | 85 | 40 | 461 | 0.7 | nd | 0.704610 |
| Pagoda | 351 | 0.84 | 3.40 | -0.33 | 191 | 14.8 | 217 | 164 | 6.01 | 25.4 | 9.5 | 220 | 361 | 54.4 | 14.0 | 11 | 466 | 830 | 32 | 20 | 461 | 0.7 | 0.2 | 0.704890 |
| Launch Pad | 351 | 4.45 | 3.21 | -0.88 | 163 | 12.4 | 170 | 123 | 5.68 | 20.8 | 4.1 | 179 | 293 | 53.7 | 13.8 | 14 | 508 | 1110 | 560 | 41 | 475 | 0.8 | 0.2 | 0.705014 |
| Bottom seawater | -1 to 0 | 53.5 | nd | 2.4 | 465 | 9.97 | 25.0 | 2.3 | 10.0 | 88.4 | 0.08 | 540 | 831 | 62.8 | nd | bdl | bdl | bdl | bdl | bdl | 420 | 0.0 | -0.1 | 0.709182 |

nd: Not determined.

bdl: Below detection limit.

* Lowest measured value.

[†] Highest measured concentration in low-Mg fluids from E9.

[‡] Highest measured concentration in low-Mg fluids from E2 and E9.

Table 3
Molar element/Cl ratios for end-member fluids from the East Scotia Ridge.

| Vent | Na/Cl | K/Cl | Li/Cl $\times 10^{-3}$ | Cs/Cl $\times 10^{-6}$ | Ca/Cl | Sr/Cl $\times 10^{-3}$ | Br/Cl $\times 10^{-3}$ | F/Cl $\times 10^{-3}$ | Mn/Cl $\times 10^{-3}$ | Fe/Cl $\times 10^{-3}$ | B/Cl $\times 10^{-3}$ |
|-----------------|-------|------|---------------------------|---------------------------|-------|---------------------------|---------------------------|--------------------------|---------------------------|---------------------------|--------------------------|
| <i>E2</i> | | | | | | | | | | | |
| Dog's Head | 0.80 | 0.07 | 1.12 | 1.13 | 0.06 | 0.19 | 1.57 | 0.07 | 3.8 | 2.4 | 0.99 |
| Sepia | 0.79 | 0.07 | 1.14 | 1.12 | 0.06 | 0.19 | 1.58 | 0.07 | 3.9 | 1.9 | 1.0 |
| Sepia Flange | 0.79 | 0.07 | 1.14 | 1.15 | 0.06 | 0.18 | 1.62 | 0.08 | 4.3 | 1.5 | 1.1 |
| <i>E9</i> | | | | | | | | | | | |
| Black & White | 0.98 | 0.07 | 1.24 | 0.66 | 0.07 | 0.23 | 1.75 | 0.35 | 2.0 | 8.1 | 4.7 |
| Ivory Tower | 0.87 | 0.07 | 0.99 | 0.75 | 0.03 | 0.12 | 1.64 | 0.18 | 2.8 | 5.5 | 2.1 |
| Pagoda | 0.87 | 0.07 | 0.99 | 0.75 | 0.03 | 0.12 | 1.64 | 0.25 | 2.1 | 3.8 | 2.1 |
| Launch Pad | 0.91 | 0.07 | 0.95 | 0.69 | 0.03 | 0.12 | 1.64 | 0.30 | 2.8 | 6.2 | 2.6 |
| Bottom seawater | 0.86 | 0.02 | 0.05 | 0.00 | 0.02 | 0.16 | 1.54 | 0.12 | nd | nd | 0.78 |

part of the chimney is dominated by medium- to coarse-grained anhydrite with only minor sulphide mineralisation. The sulphide phases are dominated by fine-grained pyrite, intergrown with minor chalcopyrite and associated with rare, fine-grained sphalerite. The sulphide minerals are present both between and within the larger anhydrite crystals. An abrupt, irregular contact, roughly parallel to the inner vent wall, marks the boundary with an outer, more sulphide-dominated mineral zone. This zone contains abundant medium grained chalcopyrite, which forms extensive granular aggregates. The chalcopyrite is intergrown with pyrite, and very small amounts of sphalerite. On the inner margin of this mineral zone, close to the contact with the gangue-rich mineral zone, pyrite is found in moderate quantities in between the other sulphide phases. However, the pyrite concentration decreases significantly towards the outer chimney wall. The chalcopyrite-rich zone grades into a layer that contains much finer grained chalcopyrite, with medium-grained anhydrite. This zone also contains fine-grained pyrite, and the chalcopyrite is occasionally intergrown with sphalerite. Sphalerite is only present as a minor phase ($\sim 3\%$), but it is significantly more abundant in this outer layer than it is in the inner parts of the chimney.

The tip of the Black & White chimney in the northern part of E9 also contains abundant anhydrite ($\sim 40\%$ to 80%), and the chimney itself has a very soft texture and is highly friable. The inner surface of the orifice of the chimney consists of medium-grained anhydrite that is mixed with minor fine-grained chalcopyrite and rare fine-grained pyrite. Occasionally, the innermost part of this anhydrite-rich zone is partially coated by a very thin (typically ~ 1 mm) layer of fine-grained chalcopyrite. This inner mineral zone is highly porous. Outside of this zone is a layer that mainly consists of fine-grained chalcopyrite, associated with minor ($< 20\%$) pyrite. This zone also contains fine- to medium-grained anhydrite, which encapsulates sulphide phases and appears to have grown around pre-existing mineral grains (Fig. 7e). This chalcopyrite-dominated layer grades into an outer, relatively porous mineral zone composed of fine-grained pyrite, which is occasionally mixed with minor quantities ($< 1\%$) of bornite. This zone is also associated with minor fine-grained sphalerite, which locally appears intergrown with both pyrite and chalcopyrite. The

pervasive anhydrite, seen within the chalcopyrite-rich layer, continues through this zone (Fig. 7e). The outermost surface of the chimney is dull grey-black in colour, and mainly consists of various sulphide minerals (marcasite, pyrite, chalcopyrite and sphalerite).

5. DISCUSSION

5.1. Controls on the chemistry of vent fluids from the East Scotia Ridge

Hydrothermal fluids are the product of chemical exchange between seawater and the ocean lithosphere at high temperature in the deepest part of the hydrothermal convection cell. Although segments E2 and E9 of the East Scotia Ridge have similar magma compositions (Fig. 2), our data reveal that the chemical composition of the vent fluids is remarkably variable. Processes in addition to water–rock reaction must therefore have a major impact on the chemical composition of the ESR fluids. These could include phase separation, magmatic degassing, cooling and mixing with seawater prior to venting, or differences in hydrologic conditions in the reaction zone (such as temperature and the water/rock ratio).

5.1.1. Phase separation and chloride variability

The Cl content of E2 vent fluids is almost identical to seawater, whereas all of the vent fluids sampled at E9 have much lower Cl (Table 2). Depletion (or enrichment) of Cl relative to seawater in vent fluids is typically attributed to phase separation (Butterfield et al., 1994; Von Damm et al., 1997; Seewald et al., 2003; Seyfried et al., 2003). The maximum temperature recorded at Black & White (383°C) lies on the two-phase boundary for seawater at this depth (Fig. 8; Bischoff and Rosenbauer, 1985), consistent with subcritical boiling at this site. Fluids from the other E9 vents, however, have measured temperatures ($348\text{--}351^\circ\text{C}$) significantly below the two-phase boundary. As their Cl content is low ($179\text{--}220$ mM), this means that extensive sub-surface cooling must occur prior to venting at the seafloor. In support of this, extrapolation of diffuse fluid temperatures at these sites to zero Mg generates higher temperatures ($363\text{--}382^\circ\text{C}$), and the upper end of this range lies on the two-phase boundary (Fig. 8).

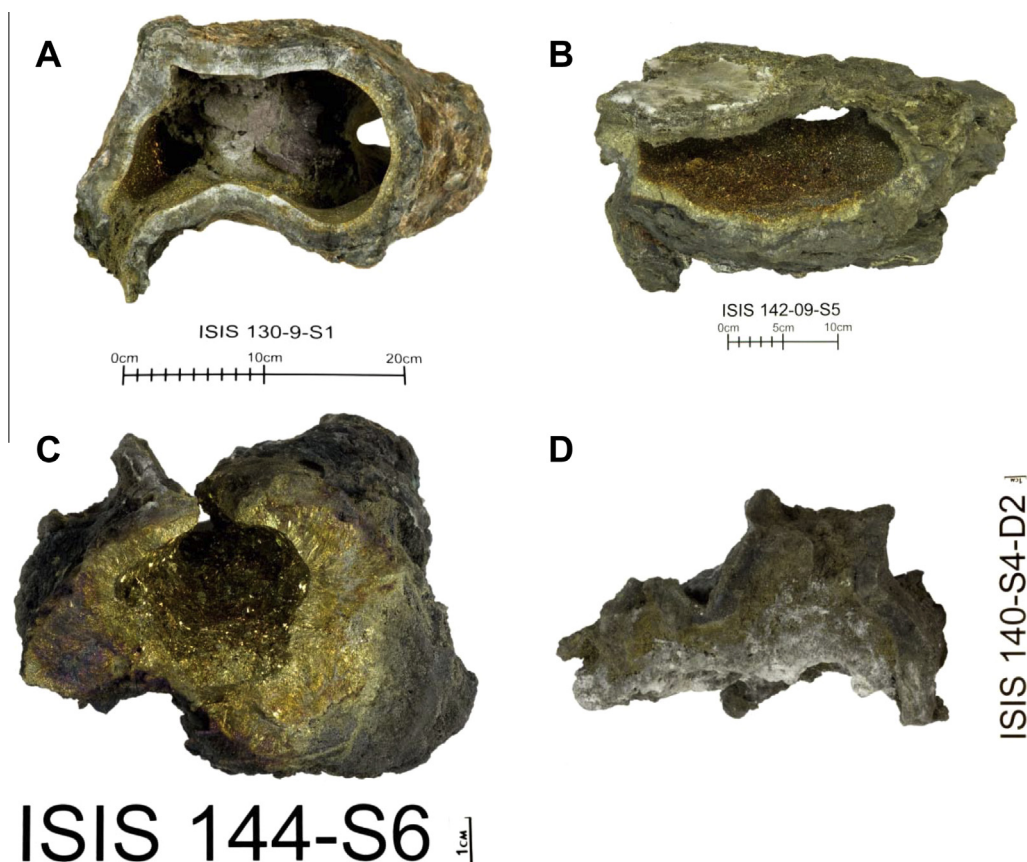


Fig. 6. Photographs of cut sections through chimney structures recovered from the East Scotia Ridge. (A) Dog's Head. (B) Ivory Tower. (C) Pagoda. (D) Black & White. Note the absence of chalcopyrite-rich phases on the inner surface of the Black & White chimney.

Low Cl fluids from E9 have higher Br/Cl (and B/Cl) than the fluids from E2 and seawater (Table 3). Experimental studies of basalt-seawater reaction at high temperature and pressure indicate that the vapour phase that forms under supercritical conditions is enriched in Br relative to Cl, while under subcritical conditions, fractionation of Br and Cl is minimal (Berndt and Seyfried, 1990). However, these experiments were conducted under closed-system conditions, and the results have not been reproduced in some other studies (e.g. Liebscher et al., 2006). More recent work, conducted under more realistic open-system conditions, indicates that Br (and B) is partitioned preferentially into the low-salinity vapour fluids under both sub- and supercritical conditions (Foustoukos and Seyfried, 2007a), which supports the idea that the Br/Cl and B/Cl ratios of E9 fluids are affected by phase separation.

5.1.2. Conditions in the sub-seafloor reaction zone

Pressure and temperature conditions in the sub-seafloor reaction zone are generally estimated from the concentration of dissolved silicon in the hydrothermal vent fluid, by assuming that dissolved silicon is controlled by quartz solubility. Although studies of quartz solubility in NaCl systems have been conducted over a wide range of pressure and temperature conditions, they are however limited in the critical region of seawater, and the effects of dissolved

chloride concentration are poorly constrained (e.g. Fournier, 1983; Von Damm et al., 1991). Experimental studies reveal that the concentration of dissolved silicon depends strongly on the density of the fluid phase, so that dissolved silicon is lower in low-density vapour-rich phases near the two-phase boundary in temperature–pressure–dissolved silicon space (Foustoukos and Seyfried, 2007b). In support of this, the low-Cl vent fluids from E9 have lower dissolved silicon than the higher Cl vent fluids from E2.

Nevertheless, the dissolved silica content of the E9 vent fluids is significantly higher than Foustoukos and Seyfried (2007b) measured in their experiments conducted at close proximity to the two-phase boundary under subcritical conditions ($[\text{Si}] = 2.2$ to 3.8 mmol/kg, with $[\text{Cl}] = 15$ – 71 mmol/kg). Rather, their experiments suggest that the low-Cl fluids sampled at E9 formed at supercritical conditions, with temperatures equal to or greater than ~ 430 °C, and pressures of ~ 320 to >360 bars (Fig. 9). This would place the reaction zone at depths of between 800 m (Black & White) and >1200 m (southern vent sites), below the seafloor.

The predicted equilibrium pressure for Dog's Head, based on quartz solubility, is ~ 350 bars (Von Damm et al., 1991), whereas the predicted equilibrium pressure for Sepia is ~ 800 bars, which implies an unreasonable reaction zone depth. A more plausible explanation is that cooling of the Sepia source fluid has occurred during upflow, as

evidenced by lower end-member Fe concentrations but higher end-member Mn concentrations (discussed below; Table 2). Nevertheless, in summary, it seems likely that the very high levels of dissolved silicon in E2 fluids corresponds to a higher pressure, higher salinity fluid ascending from the reaction zone, whereas the relatively low dissolved silicon content of the E9 fluids corresponds to a relatively low-pressure, high-temperature reaction zone.

Fluid mobile elements such as Li, Cs and B can be used to estimate water/rock ratios in hydrothermal systems if their concentrations in the rock are known (Mottl and Holland, 1978; Von Damm et al., 1985). However, as end-member B concentrations are affected by phase separation, B cannot be considered to behave as a mobile trace element at the ESR. Using data for Cs for fresh lava glasses from segments E2 and E9 (~0.15 ppm and ~0.08 ppm, respectively; Leat et al., 2000; Fretzdorff et al., 2002), and Li data for basaltic andesites (~8 ppm; Ryan and Langmuir, 1987), and assuming 100% extraction of Cs and Li from the host rock, maximum water/rock ratios are ~1.9 for E2 vents, and in the range 3.7–9.4 for E9 vents. Water–rock ratios estimated for Black & White are ~2 times higher than those estimated for the other E9 vents.

Water–rock ratios can also be estimated using $^{87}\text{Sr}/^{86}\text{Sr}$ data. Assuming that fresh lava glasses from E2 have $^{87}\text{Sr}/^{86}\text{Sr} = 0.7030$ (Leat et al., 2000) and those from E9 have $^{87}\text{Sr}/^{86}\text{Sr} = 0.7031$ (Fretzdorff et al., 2002), then according to the dissolution-precipitation model of Berndt et al. (1988), water–rock ratios are in the range 6–15 at E2, and 40–69 at E9. These ratios are much higher than those calculated from Li and Cs systematics, because of incomplete extraction of Sr and the formation of Sr-bearing secondary phases.

Despite the uncertainties in estimating water–rock ratios, all of the methods discussed above indicate that water/rock ratios are higher at E9 than they are at E2. Lower end-member $\delta^{18}\text{O}$ and δD values at the E9 vent sites also indicate that the water–rock ratio in its reaction zone is higher than it is at E2 (Shanks, 2001), and higher concentrations of Cu in E9 fluids are consistent with experimental studies which indicate that dissolved Cu is higher under more oxidising conditions, and hence higher water/rock ratios (Foustoukos and Seyfried, 2005). Considered together, these data suggest that the extent of water–rock interaction appears to be more limited at E9, which may be attributed to a shallower reaction zone and/or a shorter residence time of the fluids within the hydrothermal system (Von Damm et al., 1997).

5.1.3. Input of magmatic gases?

Segments E2 and E9 of the ESR are magmatically inflated, and it is proposed that this is the result of inflow of enriched mantle charged with volatiles from the nearby subducting slab (Livermore et al., 1997; Bruguier and Livermore, 2001). At E2, seismic reflection data indicate the existence of a magma chamber ~3 km beneath the seafloor (Livermore et al., 1997). At E9, the situation is more complex. Seismic reflection data obtained from the Devil's Punchbowl caldera indicate that a magma body existed ~2.6 km below the seafloor, which subsequently collapsed with injection of the melt into a much shallower reservoir,

<0.1 Myr ago (Bruguier and Livermore, 2001). Given that the apparent depth of quartz–fluid equilibrium for some ESR vent fluids is >1.2 km, it is possible that the circulating hydrothermal fluids may reach sufficient depths to entrain volatiles exsolved from the degassing melt lens, as observed at other vent fields on back-arc spreading ridges (e.g. the Mariner field on the Valu Fa Ridge in the Eastern Lau Spreading Centre (Mottl et al., 2011), and vent fields in the Manus Basin (Reeves et al., 2011)).

Without gas-tight samplers for this first study of hydrothermal fluids from the ESR, it is not possible to present direct evidence for magmatic degassing from helium and CO_2 data (e.g. Craig and Lupton, 1981; Marty and Jambon, 1987; Sedwick et al., 1994; Lupton et al., 2006). However, we can investigate these processes indirectly using trace elements and isotopes that are recovered faithfully from fluids collected using the Ti-syringe samplers. Magmatic fluids have extremely low δD values (–40‰ to –80‰), and $\delta^{18}\text{O}$ values of 6–8‰ (Taylor, 1979; Ohmoto, 1986). Some of the fluids recovered from the Manus Basin have unusually low δD (as low as –8.1‰), as well as relatively high $\delta^{18}\text{O}$ (up to 1.8‰) (Gamo et al., 1997; Reeves et al., 2011), and are thought to reflect mixing between hydrothermal fluids that have experienced high temperature fluid–rock interactions (which increase δD and $\delta^{18}\text{O}$: Bowers and Taylor, 1985; Bowers, 1989; Shanks et al., 1995; Shanks, 2001) and magmatic H_2O (Gamo et al., 1997; Reeves et al., 2011). By contrast, the end-member vent fluids from both ESR segments have slightly positive δD (0.2–1.1‰), and $\delta^{18}\text{O}$ values (0.5–1.1‰) are not substantially different from seawater (0.0‰). However, fluids venting at the Mariner field on the Valu Fa Ridge (Eastern Lau Spreading Center), which are also thought to be affected by input of magmatic gases, do not exhibit low δD (–1.3‰ to 1.9‰, relative to –3.2‰ in bottom seawater; Mottl et al., 2011). In addition to high temperature fluid–rock interactions, D may be enriched in vapour-rich fluids affected by phase separation (Berndt et al., 1996; Foustoukos and Seyfried, 2007c). Thus, although it seems that significant input of magmatic gases to ESR vent fluids is unlikely, we cannot preclude the possibility that a magmatic δD signal has been overprinted by hydration reactions between fluids and crust at low water–rock ratios (E2 and E9), and/or phase separation processes (E9).

Vent fluids affected by input of magmatic volatiles also tend to have low pH, and high concentrations of F, relative to fluids venting from mid-ocean ridges (e.g. Gamo et al., 2006; Reeves et al., 2011). The pH of the ESR fluids (3.0–3.4) is at the lower end of the range for high temperature vent fluids from MOR hydrothermal systems (2.6–4.4; Butterfield et al., 2003), but is generally higher than the pH of >250 °C vent fluids thought to be affected by input of magmatic fluids in other back-arc basin settings (2–3; Gamo et al., 1997; Mottl et al., 2011; Reeves et al., 2011). Similarly, F concentrations in ESR end-member fluids are within the range measured in MOR hydrothermal systems, where F is depleted relative to seawater (Edmond et al., 1979; Maris et al., 1984; Von Damm et al., 1985; Seyfried and Ding, 1995; German and Von Damm, 2003). Fluids affected by magmatic inputs tend to be enriched in F

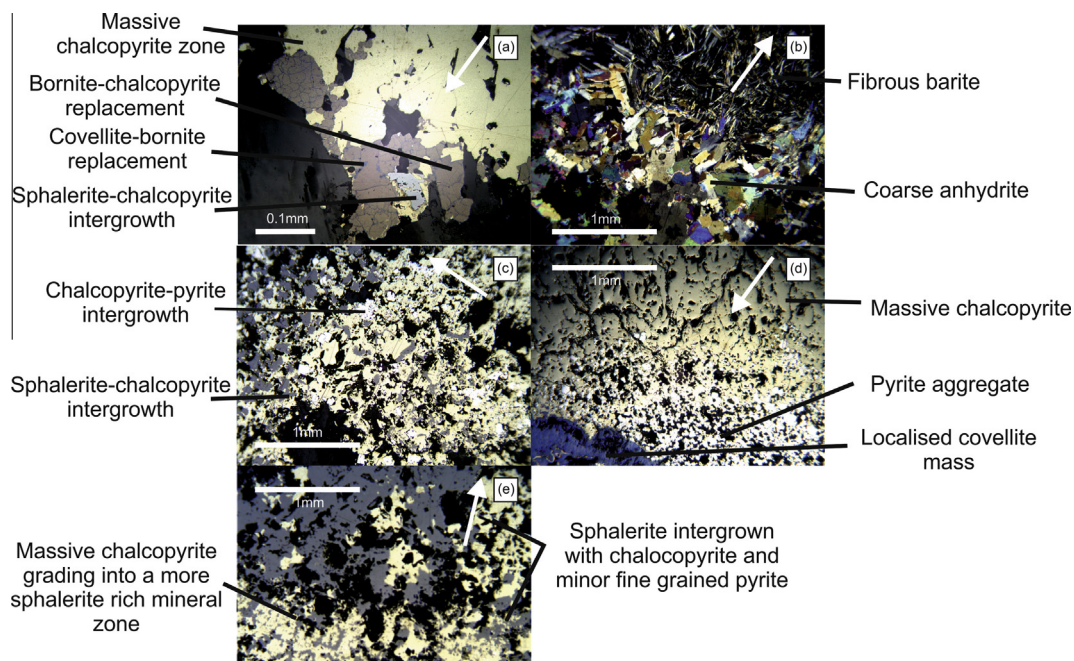


Fig. 7. Photomicrographs of thin sections of chimney structures from the East Scotia Ridge, showing typical patterns of mineral zonation. Arrows point to the exterior of the chimney wall. (a) Section through the orifice at Dog's Head (E2), showing the inner, chalcopyrite-rich zone, with intergrowth between chalcopyrite and bornite in the outer part of this layer. The bornite tends to be replaced by covellite along grain boundaries. Reflected light. (b) Outer part of the chimney wall at Dog's Head, showing the transition from coarse-grained anhydrite to a barite dominated zone, which extends to the outermost part of the orifice. Cross-polarised light. (c) Section through a chimney from Ivory Towers (E9) showing the innermost massive chalcopyrite-rich layer. Note that the outer part of this zone becomes more fine-grained, and the chalcopyrite becomes intergrown with sphalerite. Reflected light. (d) Section through a chimney from Pagoda (E9), showing the inner chalcopyrite-rich layer, and the presence of covellite in the outer part of the layer. Reflected light. (e) Section through the chalcopyrite-rich layer, which surrounds the innermost anhydrite-rich layer, of a chimney from Black & White (E9). The outer part of this zone becomes increasingly sphalerite rich. Reflected light.

relative to seawater (Mottl et al., 2011; Reeves et al., 2011). Interestingly, the F/Cl ratio of fluids from E9 ($0.18 \times 10^{-3} - 0.35 \times 10^{-3}$) is higher than that of seawater (0.12×10^{-3}) (Table 3), and within the range reported for the Manus Basin and Mariner vent fields (respectively, $0.19 \times 10^{-3} - 0.93 \times 10^{-3}$ and $0.12 \times 10^{-3} - 0.21 \times 10^{-3}$) that are thought to be affected by magmatic inputs (Mottl et al., 2011; Reeves et al., 2011). This may be due to enrichment of F in the vapour phase during phase separation, although there is only a weak correlation ($r^2 = 0.3$) between Cl and F/Cl based on the data reported in Reeves et al. (2011) and Mottl et al. (2011), and the behaviour of F in submarine hydrothermal systems is poorly understood (Seyfried and Ding, 1995). Rock leaching has also been proposed as a source of F to some felsic-hosted terrestrial geothermal systems (Arnorsson et al., 1978), although, as Reeves et al. (2011) point out, the F contents of unaltered dacites from the Paul Ridge in the Manus Basin are not substantially different from typical MORB.

On balance, there is no compelling evidence for magmatic degassing into the hydrothermal systems at E2 and E9, despite seismic evidence for the existence, or recent existence, of a magma chamber underneath both segments. If the magma chamber is degassing, then the volatiles must be prevented from interacting with the hydrothermal fluids, perhaps due to the presence, or absence, of extensive

faulting. Alternatively, the abundance of magmatic volatiles may be low. In support of this, the water content of volcanic glasses recovered from segments E2 and E9 (0.30–1.02 wt%; Fretzdorff et al., 2002) is slightly lower than it is in glasses recovered from the Manus Basin (1.2 to 1.8 wt%; Sinton et al., 2003) and the Valu Fa Ridge on the Eastern Lau Spreading Center (1.3 wt%; Fouquet et al., 1993), on segments that host vent fluids thought to be affected by input of magmatic volatiles.

5.1.4. Influence of sub-surface processes

Concentrations of Mg in the high-temperature samples are very low, suggesting that they have not mixed substantially with seawater prior to venting. Unusually, the Fe concentration in E2 end-member fluids is much lower than the end-member Mn concentration (Table 2). As Fe preferentially precipitates relative to Mn on cooling (Seyfried and Ding, 1993), this suggests that the E2 fluids have cooled during upflow; the Sepia flange fluids appear to have undergone additional cooling as they have even higher Mn/Fe ratios.

Cooling reduces both the stability of iron chloride complexes and the solubility of iron and iron-copper sulphides, resulting in removal of Fe and Cu from solution. Precipitation of iron and iron-copper sulphides generates acidity (see Reeves et al., 2011), which may explain why the pH of high

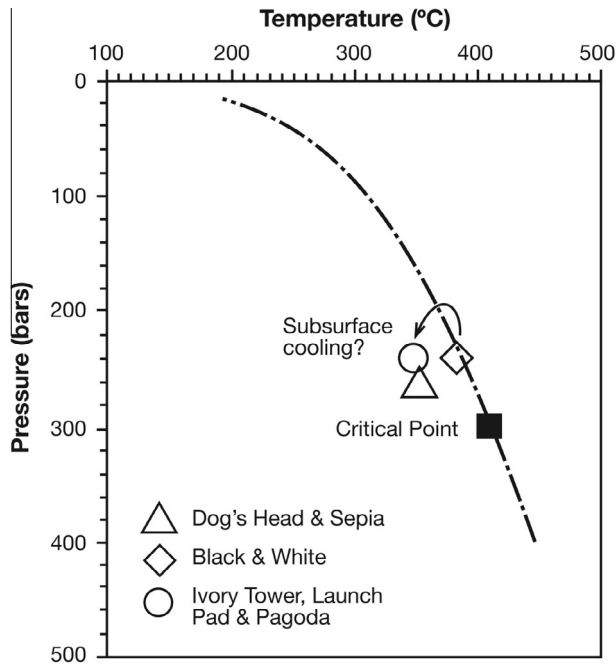


Fig. 8. Maximum measured vent fluid temperature vs. seafloor pressure for vent sites on the ESR. The dashed black line shows the two-phase boundary for a 3.2 wt% NaCl solution, and the black square shows the critical point of seawater (from Bischoff and Rosenbauer, 1985). Fluids from Ivory Tower, Launch Pad and Pagoda may have cooled during transport to the seafloor (curved arrow; see text for details).

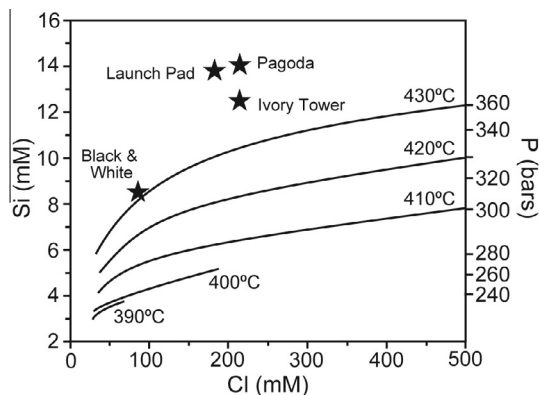


Fig. 9. Dissolved silicon and Cl concentrations measured in vapour-rich fluids at E9, in comparison with quartz solubility data modelled by Foustoukos and Seyfried (2007b), based on their experimental data. Dissolved silicon concentrations suggest that the low-Cl vent fluids formed at higher temperature and pressure than the critical point of seawater (see Fig. 8).

temperature fluids from E2 is slightly lower than the pH of E9 end-member fluids (Table 2). Edmond et al., 1995 suggest lowering of pH promotes the remobilization of Zn from sphalerite; this is consistent with higher Zn in E2 end-member fluids, although Cl concentration appears to be the principal control on Zn in ESR vent fluids.

5.2. Controls on hydrothermal mineralisation

The morphology and mineralogy of the uppermost part of active black smoker chimneys collected at the ESR are summarised in Fig. 10. Chimney material from E2 (Dog's Head), Ivory Tower and Pagoda, typically exhibits inner zones of massive chalcopyrite enclosed within an outer zone of disseminated sulphide, principally sphalerite and pyrite, in an anhydrite matrix. At E2, barite becomes the dominant sulphate mineral towards the outermost part of the chimney wall. Bornite may be present in the outermost part of the outer zone, where it appears to replace chalcopyrite. In turn, bornite may be replaced by covellite. Sphalerite tends to be less abundant in the E2 chimneys, whereas bornite and covellite are more common. By contrast, the innermost part of the chimneys recovered from the northern vent site at E9 (Black & White), and Launch Pad on the southern section of E9, are dominated by anhydrite.

The pattern of mineral zonation that we observe is similar to other high-temperature black smoker chimneys recovered from sediment-starved MOR vent sites (e.g. Haymon, 1983; Graham et al., 1988; Fouquet et al., 1988; Koski et al., 1994; Tivey, 1995). Chimney walls are initially constructed upwards from the seafloor by anhydrite precipitation from seawater which is heated to supersaturation with respect to CaSO_4 around the margins of the discharging jet of hydrothermal fluid. Hydrothermal fluid is trapped within the anhydrite or leaks into the exterior by dissolution of anhydrite along cleavage planes. Sulphides precipitate from the hydrothermal fluids, with higher temperature mineral phases (e.g. chalcopyrite) precipitating closer to the orifice, and lower temperature mineral phases (sphalerite, pyrite) precipitating closer to the exterior (Haymon, 1983; Koski et al., 1994). The anhydrite-rich interior of the Black & White and Launch Pad chimneys is thus consistent with new chimney growth.

Once the anhydrite walls are in place, hydrothermal fluid is protected from extensive mixing with seawater and chalcopyrite begins to grow in the centre of the chimney where the temperature is highest. The hydrothermal fluids migrate outwards, progressively dissolving the anhydrite and replacing it with sulphides (mainly sphalerite, pyrite and chalcopyrite). As the fluid moves towards the exterior of the chimney, conditions become more oxidising, resulting in replacement of bornite with covellite and the precipitation of more sulphur-rich phases such as pyrite (Haymon, 1983; Graham et al., 1988). The mineral zonation that we observe in the E2, Ivory Tower and Pagoda chimneys is thus consistent with a more mature stage of chimney growth.

As we have only sampled the uppermost section of the ESR hydrothermal chimneys, which is unlikely to be representative of the overall character of hydrothermal deposits (which also include the lower parts of the chimneys, flange structures, and sulphide platforms), we can make only general inferences about the relationships between vent fluid chemistry and mineralisation. Most notably, the overall higher abundance of barite in the outermost parts of the chimney material sampled at E2 is consistent with higher levels of Ba in the E2 vent fluids ($\sim 20 \mu\text{mol/kg}$ vs.

~ 7 $\mu\text{mol}/\text{kg}$ in E9 fluids). In this connection, the average Ba content of volcanic glasses sampled from E2 (120 ± 52 ppm; [Leat et al., 2000](#); [Fretzdorff et al., 2002](#)) is higher than it is in glasses from E9 (65 ± 22 ppm; [Fretzdorff et al., 2002](#); [Leat et al., 2004](#)).

Sphalerite is distinctly less abundant in chimney material recovered from Dog's Head relative to that recovered from the E9 sites, which may contribute to higher levels of Zn in the Dog's Head vent fluids. Similarly, limited deposition of chalcopyrite in the Black & White and Launch Pad chimneys may be at least partly responsible for high concentrations of Cu in their conjugate vent fluids. Thermodynamic considerations indicate that the high temperature (383 °C) of Black & White fluids minimizes precipitation of copper minerals (e.g. [Seewald and Seyfried, 1990](#)), but we note that the temperature of fluids from Launch Pad (351 °C) is not significantly higher than the other vent sites (348 – 353 °C) that have lower Cu.

5.3. Comparison with other hydrothermal systems

The East Scotia Ridge is the first back-arc basin hydrothermal system to have been sampled outside of the western Pacific. Compared to high-temperature hydrothermal fluids from other locations, the chemistry of ESR fluids is generally similar to fluids from other back-arc basin and MOR settings sampled at similar temperatures, and with comparable Cl concentrations ([Table 4](#)). However, fluids from back-arc basin settings that are thought to be affected by input of magmatic volatiles (Fenway, Roman Ruins and DESMOS in the Manus Basin, and Mariner and Vai Lili on the Eastern Lau Spreading Centre) have notably higher F, and lower pH, as discussed in [Section 5.1](#). Fluids collected from <1 m above degassing magma from an erupting submarine volcano (NW Rota-1) have similarly low pH (~ 1.1 ; [Butterfield et al., 2011](#)).

There are a number of other features in the data in [Table 4](#) that also call for discussion. Firstly, levels of H_2S in ESR fluids follow the overall trend with Cl for back-arc basin fluids ([Fig. 11a](#)), although E9 fluids have high H_2S relative to low-Cl fluids from the North Fiji Basin. Nevertheless, the E9 fluids do not have especially high H_2S compared to MOR fluids with similar levels of Cl. Some of the back-arc basin sites that are thought to be affected by inputs of magmatic volatiles have high H_2S relative to Cl (e.g. Fenway and DESMOS), whereas others do not (e.g. Roman Ruins and Mariner). Fluids recovered from NW Rota-1 have extremely low

H_2S (0.001 mM; [Butterfield et al., 2011](#)). High-temperature magmatic gases contain high levels of SO_2 , which is highly soluble in water. Aqueous SO_2 is unstable under hydrothermal conditions, and either rapidly hydrates to form sulphurous acid, or disproportionates to yield H_2SO_4 and either S^0 (zero-valent sulphur) or H_2S . As formation of H_2S is favoured at higher temperatures, slightly higher pH, and lower SO_2 ([Butterfield et al., 2011](#); [Reeves et al., 2011](#)), this provides a possible explanation for variable H_2S levels in back-arc basin fluids.

Concentrations of Li are closely correlated with Cl in back-arc basin vent fluids ([Fig. 11b](#)), although fluids from the Okinawa Trough have rather higher Li due to secondary interaction with overlying sediments prior to venting at the seafloor ([Gamo, 1995](#)). Fluids from the Mariner and Vai Lili vent sites on the Eastern Lau Spreading Centre have slightly lower levels of Li relative to Cl. As discussed in [Section 5.1](#), this may indicate that the extent of water–rock interaction is more limited in the reaction zone at these sites. By contrast, the overall correlation between K (and B) and Cl in vent fluids from back-arc basin settings is rather poor ([Fig. 11c](#)). This is partly because concentrations of K and B in fluids from the Okinawa Trough are unusually high, because of interactions with the overlying sediments ([You et al., 1994](#); [Gamo, 1995](#)), but also because on closer inspection of the data, it is apparent that basalt-hosted vent sites (Vienna Woods and Kilo Moana, and MORB-hosted MOR vent sites) tend to have fluids with relatively low K, whereas vent sites hosted in dacite (Fenway, Roman Ruins) and (probably, because of difficulties in isolating the input from overlying sediments) rhyolite (Yonaguni Knoll) have relatively high K. Similarly, these dacite- and rhyolite-hosted vent sites tend to have fluids with relatively high B. This is consistent with higher K and B in more silicic rocks (e.g. [Peccerillo and Taylor, 1976](#)), and the increased influence of recycled slab material ([Spivack and Edmond, 1987](#); [Ryan and Langmuir, 1993](#)). Thus, in the case of K, and probably B, it is clear that the chemical composition of the host substrate can play an important control on the composition of the vent fluids in back-arc basin settings.

Ba and Sr are expected to be enriched in back-arc basin lavas because of input of recycled slab material (e.g. [Pearce and Peate, 1995](#)). There is no obvious evidence for relatively higher Sr or Ba in back-arc basin fluids (e.g. [Fig. 11d](#)), although as discussed in [Section 4.1](#), this may be because concentrations of Ba and Sr are affected by precipitation or dissolution of, respectively, barite and anhydrite. In

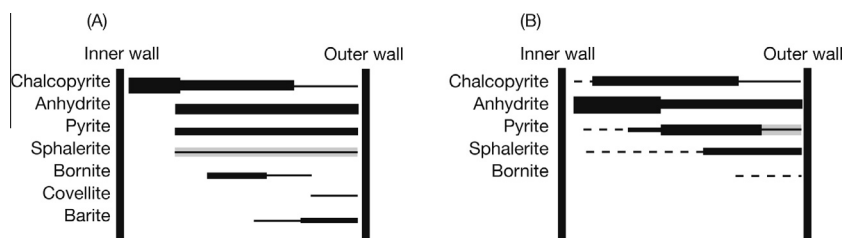


Fig. 10. Generalized pattern of mineral zonation for hydrothermal chimneys from: (A) Dog's Head, Ivory Tower and Pagoda. (B) Black & White and Launch Pad. The thickness of each bar represents the relative abundances of the mineral phases, from the inner to the outer part of the chimney orifice. Dashed lines indicate phases that are not always present; the grey shading indicates varying abundance between different chimneys.

Table 4

End-member composition of vent fluids from other back-arc basins, and MOR sites in the Atlantic, Pacific and Indian Oceans located closest to the ESR. Data are from: North Fiji Basin: Grimaud et al. (1991), Eissen et al. (1994), Ishibashi et al. (1994). Manus Basin: Gamo et al. (1997), Sinton et al. (2003), Reeves et al. (2011). Eastern Lau Spreading Centre: Fouquet et al. (1993), Pearce et al. (1995), Mottl et al. (2011). Mariana Trough: Tian et al. (2005), Gamo et al. (2006), Kakegawa et al. (2008), Kato et al. (2012), Nakamura et al. (2013). Okinawa Trough: Shinjo et al. (1999), Nakagawa et al. (2005), Suzuki et al. (2008), Kawagucci et al. (2011, 2013). Southern Mariana Arc: Embley et al. (2006), Butterfield et al. (2011). Southern Mid-Atlantic Ridge: Koschinsky et al. (2008), Schmidt et al. (2011). Central Indian Ridge: Gallant and Von Damm (2006), Kumagai et al. (2008), Nakamura et al. (2009). Southern East Pacific Rise: Von Damm et al. (2003). Data have been converted from mol/kg to mol/L (M) or vice versa where necessary.

| Site | Vent | Substrate | Max T °C | pH | Alk mEq/ L | Na mmol/ kg | K mmol/ kg | Li μmol/ kg | Cs nmol/ kg | Ca mmol/ kg | Sr μmol/ kg | Ba μmol/ kg | Cl mM | Br μM | F μM | Si mM | H ₂ S mM | Mn μmol/ kg | Fe μmol/ kg | B μmol/ kg | δ ¹⁸ O | δD | ⁸⁷ Sr/ ⁸⁶ Sr |
|------------------------------|-----------------------------|---------------------------------------|-------------|------|------------------|-------------------|------------------|-------------------|-------------------|-------------------|-------------------|-------------------|----------|----------|---------|----------|------------------------|-------------------|-------------------|------------------|-------------------|------|------------------------------------|
| <i>Back-arc basin</i> | | | | | | | | | | | | | | | | | | | | | | | |
| North Fiji Basin | White Lady | Low to med K basalt | 285 | 4.7 | 0.12 | 210 | 10.5 | 200 | nd | 6.5 | 30 | 5.9 | 259 | 311 | nd | 14.2 | 2.1 | 12 | 15 | 465 | nd | nd | 0.7046 |
| | Kaiyo | Low to med K basalt | 291 | 4.7 | -0.87 | 239 | 14.5 | 282 | nd | 9 | 43 | 5.3 | 272 | 414 | nd | 13.5 | 4.2 | 26 | 8.8 | 475 | nd | nd | nd |
| Manus Basin | Vienna Woods | Low K basalt | 282 | 4.4 | nd | 513 | 21.2 | 1080 | 291 | 80.1 | 242 | nd | 721 | 1110 | 20 | 16 | 1.4 | 351 | 150 | 236 | 0.56 | 2.4 | 0.70435 |
| | Fenway 3 | Med K dacite | 358 | 2.7 | nd | 397 | 76.1 | 917 | 2650 | 22.3 | 95.9 | nd | 582 | 914 | 178 | 12.6 | 18.8 | 3800 | 1180 | 1610 | 1.4 | -1 | 0.70394 |
| | Roman Ruins 4 | Med K dacite | 341 | 2.6 | nd | 497 | 82.1 | 1090 | 2440 | 23.1 | 86.9 | nd | 685 | 1080 | 131 | 19.8 | 6.8 | 3020 | 6860 | 1700 | 1.1 | -2.7 | 0.70425 |
| | DESMOS† | Med K basaltic andesite | 88 | 2 | -18 | 351 | 10.2 | nd | nd | 3.75 | nd | nd | 453 | nd | nd | 10.2 | 15.6 | nd | nd | nd | nd | -8.1 | nd |
| Eastern Lau Spreading Centre | Kilo Moana 1 | Low K basalt | 333 | 3.6 | -0.37 | 486 | 16.9 | 875 | 106 | 34.9 | 118 | nd | 602 | 916 | 10.8 | 19.7 | 6.2 | 512 | 2490 | 535 | 0.82 | 2.2 | 0.70446 |
| | ABE 1 | Low K basaltic andesite | 309 | 4.3 | -0.34 | 430 | 24.6 | 646 | 390 | 39.1 | 115 | nd | 553 | 880 | 13.5 | 17.7 | 3.7 | 468 | 268 | 698 | 0.86 | -1 | 0.70422 |
| | Mariner 3 | Low K basaltic andesite/andesite | 363 | 2.7 | -2.25 | 439 | 36.9 | 385 | 735 | 43.8 | 162 | nd | 629 | 1010 | 74.2 | 15.7 | 9.7 | 5720 | 13000 | 1110 | 0.35 | 0.2 | 0.70419 |
| | Vai Lili 3 | Low K basaltic andesite/andesite | 334 | 2 | nd | 561 | 75 | 593 | 1480 | 39.3 | 19 | nd | 790 | 1140 | nd | 14.5 | nd | 6800 | 2400 | 790 | nd | nd | 0.7044 |
| Mariana Trough | Alice Spring | Low K basalt/basaltic andesite | 287 | 3.9 | 0.1 | 423 | 46.4 | nd | nd | 21.3 | nd | nd | 544 | nd | nd | 14 | 2.5 | 285 | 6.2 | nd | nd | nd | nd |
| | Archaeon | Low K andesite | 343 | 3 | -1.68 | 330 | 30.4 | 504 | nd | 17.8 | nd | 52.4 | 432 | 738 | nd | 17 | 5.8 | 1180 | 2710 | 1170 | nd | nd | nd |
| Okinawa Trough | Urashima | Low K andesite | 326 | 3.01 | -1.42 | 456 | 37 | 764 | nd | 31.9 | nd | nd | 648 | nd | nd | 16.2 | 2.5 | 2220 | 554 | nd | nd | nd | nd |
| | Yonaguni Knoll (Tiger top) | Med K dacite/rhyolite | 328 | 6.7 | nd | 433 | 90.1 | nd | nd | 26.1 | nd | nd | 661 | nd | nd | 13.7 | nd | 1250 | 200 | 4310 | nd | nd | nd |
| | Yonaguni Knoll (Tiger base) | Med K dacite/rhyolite | 310 | 6.8 | nd | 254 | 55.3 | nd | nd | 14.3 | nd | nd | 385 | nd | nd | 12.8 | nd | 700 | 100 | 2930 | nd | nd | nd |
| | Iheya North Knoll (1)‡ | Low to med K basalt/basaltic andesite | 310 | 4.8 | 1.22 | 406 | 72.5 | 1220 | nd | 20 | 69.5 | nd | 552 | nd | nd | 12.7 | 4.6 | 645 | nd | 1780 | nd | nd | nd |
| | Iheya North Knoll (2)‡ | Low to med K basalt/basaltic andesite | 309 | 4.7 | 1.51 | 444 | 66 | 1150 | nd | 23.1 | 82 | 34 | 638 | nd | 189 | 13.2 | 3.7 | 702 | 116 | 1990 | 1.12 | -0.4 | nd |

(continued on next page)

Table 4 (continued)

| Site | Vent | Substrate | Max T °C | pH | Alk L | Na mmol/kg | K mmol/kg | Li mmol/kg | Cs mmol/kg | Ca mmol/kg | Sr μmol/kg | Ba μmol/kg | Cl mM | Br μM | F μM | Si mM | H ₂ S mM | Mn μmol/kg | Fe μmol/kg | B μmol/kg | δ ¹⁸ O ‰ | δD ‰ | ⁸⁷ Sr/ ⁸⁶ Sr |
|-----------------------------|----------------------------|------------------------------------|----------|-----|-------|------------|-----------|------------|------------|------------|------------|------------|-------|-------|------|-------|---------------------|------------|------------|-----------|---------------------|------|------------------------------------|
| <i>Back-arc basin</i> | | | | | | | | | | | | | | | | | | | | | | | |
| <i>Arc Volcano</i> | | | | | | | | | | | | | | | | | | | | | | | |
| Southern Mariana Arc | NW Rota-1 | Med K basalt/ basaltic andesite | 201 | 1.1 | nd | nd | 9.15 | nd | nd | 11.9 | nd | 4.1 | nd | nd | nd | 7.03 | 0.001 | 114 | 2740 | nd | nd | 0.5 | nd |
| <i>MOR</i> | | | | | | | | | | | | | | | | | | | | | | | |
| Southern Mid-Atlantic Ridge | Sisters Peak | MORB | 400 | nd | nd | 209 | 7.4 | 343 | nd | 14.5 | 43.5 | nd | 224 | 392 | nd | 14.4 | 8.3 | 704 | 3380 | 591 | nd | nd | nd |
| | Red Lion | MORB | 349 | nd | nd | 480 | 19.8 | 1220 | nd | 18.6 | 63.1 | nd | 552 | 873 | nd | 21.8 | nd | 730 | 803 | 520 | nd | nd | nd |
| | Nibelungen | Ultramafic | 372 | 2.9 | nd | 449 | 18.6 | 391 | 250 | 30.9 | 84.8 | 27.8 | 567 | 894 | nd | 13.7 | 1.1 | 962 | 5240 | 192 | 2.24 | 7.6 | nd |
| | Kairei (6) | MORB/ultramafic | 365 | 3.4 | -0.32 | 530 | 15.2 | 545 | nd | 31.3 | 79.6 | nd | 620 | 970 | nd | 16.7 | 3.9 | 857 | 6010 | nd | nd | nd | nd |
| | Edmond (A) | MORB | 382 | 3.1 | -0.53 | 725 | 44.2 | 1050 | nd | 63.4 | 184 | nd | 927 | 1390 | nd | 20.8 | 4.8 | 1430 | 13900 | nd | nd | nd | nd |
| | Southern East Pacific Rise | MORB | 401 | 3.1 | -0.82 | 248 | 6.87 | 270 | nd | 15.8 | 47.2 | nd | 297 | 490 | nd | 8.69 | 7.9 | 622 | 6970 | 429 | 0.77 | 1.7 | nd |
| | Brandon (Bb.3) | MORB | 368 | 3.2 | -0.71 | 451 | 13.4 | 489 | nd | 97.6 | 97.6 | nd | 558 | 880 | nd | 12.1 | 6.7 | 1300 | 12500 | 462 | 0.7 | 1.1 | nd |

nd: Not determined.

* Units mmol/kg.

† End-member assumed to have [Mg] = 49 mmol/kg.

‡ (1) Average of data collected in 1997 and 2007; (2) Data collected 18 months after IODP drilling.

support of this, fluids from back-arc basin settings tend to have higher ⁸⁷Sr/⁸⁶Sr ratios (Table 4) relative to fluids from mid-ocean ridges (0.7028–0.7041; Von Damm, 1990), which reflects the generally higher ⁸⁷Sr/⁸⁶Sr ratio of back-arc lavas (e.g. 0.70250–0.70348 on the East Scotia Ridge; Fretzdorff et al., 2002) by comparison with normal MORB (0.70264 ± 0.00022; Ito et al., 1987).

As discussed in Section 5.2, the mineralogy of the uppermost sections of the chimneys recovered from the ESR is similar to chimneys on sediment-starved MOR hydrothermal sites. Chimney material from the White Lady hydrothermal site in the North Fiji Basin is similarly dominated by Cu-, Fe-, and Zn-rich sulphides, and anhydrite, and, like E2, the deposits are slightly enriched in Ba (Bendel et al., 1993). However, chimney material recovered from Vai Lili, on the Eastern Lau Spreading Centre, and from the Mariana Trough, is substantially different from that recovered from the ESR and the North Fiji Basin, in that it is dominated by barite and anhydrite is sparse (Moore and Stakes, 1990; Fouquet et al., 1993). The Vai Lili mineralisation also has distinctly higher Zn and lower Fe, as well as higher As, Pb, Ag, Au and Hg concentrations, and lower amounts of Mo, Se, and Co, relative to mid-ocean ridge deposits (Fouquet et al., 1993).

Chimneys venting high temperature (325–328 °C), high Cl (614–635 mmol/kg) fluids at the Yonaguni Knoll IV hydrothermal field in the Okinawa Trough back-arc basin are either anhydrite-rich, with sulphide disseminations in the anhydrite, like Black & White and Launch Pad, or they are mainly composed of barite with sulphide disseminations (Suzuki et al., 2008), like Vai Lili and the Mariana Trough. By contrast, chimney material recovered from the Crystal site at Yonaguni Knoll IV, which vent lower temperature (220 °C) fluids that are thought to be vapour-rich, are characterised by carbonates including calcite and magnesite, and Mn-bearing sulphides including alabandite, sphalerite and fahlore (Suzuki et al., 2008). Although the presence of calcite has been reported for a number of sediment-hosted hydrothermal systems (e.g. Koski et al., 1985), these authors suggest that the Mn-rich signature of the sulphides may be characteristic of chimneys forming from vapour-rich hydrothermal fluids, due to enrichment of Mn relative to Fe and Zn. However, Mn-sulphide phases are not observed in the chimney samples from Black & White and Launch Pad, nor are they observed in chimneys venting low-Cl fluids at the Virgin hydrothermal site on Axial Seamount, Juan de Fuca Ridge (which consist of anhydrite with highly variable levels of impregnation by pyrite and sphalerite; Harvey-Kelly et al., 1988). Moreover, low-Cl vent fluids from E9 have lower Mn/Cl, and higher Fe/Cl, relative to the higher-Cl fluids from E2. Although our data, together with those from Axial Seamount, suggest that venting of low-Cl fluids may promote precipitation of sulphates (anhydrite) in preference to sulphides, the role of phase separation on the mineralogy of hydrothermal chimneys is, as yet, unclear.

6. SUMMARY AND CONCLUSIONS

Analyses of the chemical and isotopic compositions of high temperature hydrothermal vent fluids and associated

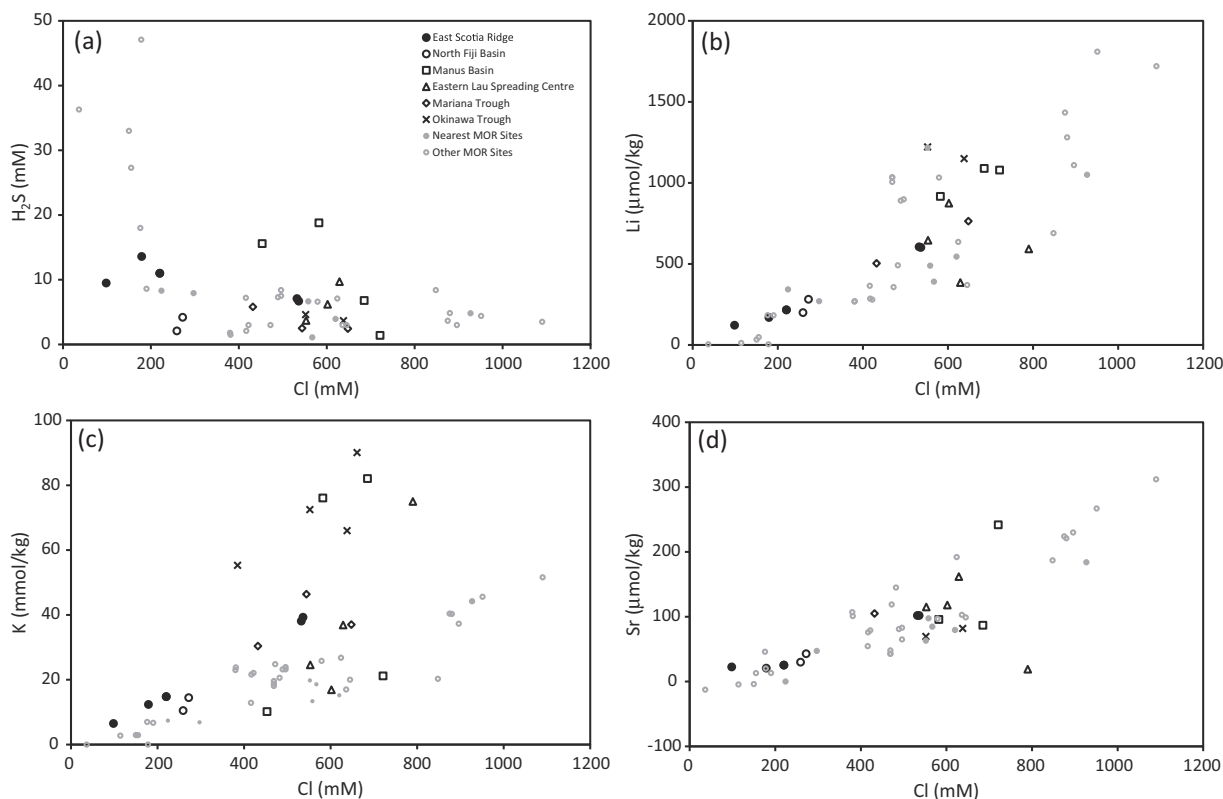


Fig. 11. Concentration of Cl vs. (a) H_2S , (b) Li, (c) K and (d) Sr, in end-member fluids from various back-arc basin settings, as well as from a selection of MOR hydrothermal sites. Nearest MOR sites are given in Table 4. Other MOR sites are: 21°N East Pacific Rise (Von Damm, 1990); 9–10°N East Pacific Rise (Von Damm, 2000), 17–19°S East Pacific Rise (Charlou et al., 1996); Axial Seamount, Juan de Fuca Ridge (Butterfield et al., 1990); North Cleft, Juan de Fuca Ridge (Butterfield and Massoth, 1994); Southern Juan de Fuca Ridge (Von Damm and Bischoff, 1987); Lucky Strike, Mid-Atlantic Ridge (Charlou et al., 2000); Menez Gwen, Mid-Atlantic Ridge (Charlou et al., 2000); Broken Spur, Mid-Atlantic Ridge (James et al., 1995); and TAG, Mid-Atlantic Ridge (Edmonds et al., 1996).

mineralisation from the ESR, reveal significant variations both between and within ridge segments. Vent fluids recovered from the E9 segment have very low levels of Cl, the lowest measured in any fluids recovered from a back-arc spreading centre to date, and must result from phase separation within the sub-seafloor hydrothermal convection cell. Differences in the concentrations of most cations in the vent fluids can largely be explained by differences in vent fluid Cl, due to charge balance constraints. Important exceptions are copper and iron, which have significantly lower metal/Cl ratios in the higher Cl vent fluids sampled from segment E2. The concentration of these elements appears to reflect either cooling of the fluids in the hydrothermal upflow zone, or less oxidising conditions (lower water/rock ratios) in the reaction zone. Concentrations of fluid mobile elements indicate that water/rock ratios are ~ 2 –4 times greater in the reaction zone at E9, compared to E2.

Although seismic work indicates that both segments E2 and E9 are magmatically inflated, we find no compelling evidence for input of magmatic volatiles in the vent fluids. This suggests that either the volatiles are prevented from interacting with the hydrothermal fluids, or their abundance is low. In support of the latter, the water content

of volcanic glasses from the ESR is generally lower than it is in lavas from back-arc basin settings that host vent fluids thought to be affected by magmatic input.

The pattern of mineral zonation in the uppermost sections of chimneys that vent high-temperature fluids at the ESR is generally similar to that observed at sediment-starved MOR hydrothermal sites. Nevertheless, the anhydrite content of the interior of chimneys that issue fluids with the lowest Cl (Black & White and Launch Pad) is distinctly higher than it is in chimney material recovered from the other sites. This may indicate either that the tips of the Black & White and Launch Pad chimneys formed very recently, or that low-Cl fluids promote precipitation of sulphate phases in preference to sulphides.

Considered together with existing data, it is clear that the chemical composition of hydrothermal fluids sampled from back-arc settings shows many similarities, but also important differences, to fluids issuing from mid-ocean ridges. Back-arc basin fluids can be affected by inputs of magmatic volatiles, but this seems to be the exception rather than the rule, even where there is seismic evidence for the existence, or recent existence, of a magma chamber underneath the vent fields, as there is at E2 and E9. Rather more commonly, back-arc basin fluids have relatively high

levels of K and B, and higher $^{87}\text{Sr}/^{86}\text{Sr}$, which reflects the input of recycled slab material. For the same reason, the abundance of barite in chimney material is also generally higher in back-arc basin settings. Nevertheless, whatever the tectonic setting, the concentration of Cl is the dominant control on the concentration of most chemical species in hydrothermal fluids.

ACKNOWLEDGEMENTS

We thank the captain and crew of RRS *James Cook*, and the ISIS ROV team, on cruise JC42 for their critical support in the collection of these samples. Matt Cooper is thanked for assistance with the Sr isotope analyses, and Gregor Hsiao, Lisa Munro, Kim Law, and Li Huang are all thanked for help with stable isotope analyses of the fluids. We gratefully acknowledge constructive comments from three anonymous reviewers, which have helped to improve the manuscript. This work was funded by the Natural Environment Research Council consortium grant NE/D01249X/1. C.R.G. acknowledges further support from the National Science Foundation's Office of Polar Programs grant ANT-0739675. N.R.B. acknowledges funding from the National Sciences and Engineering Research Council of Canada, Ontario Ministry of Research and Innovation, and the Academic Development Fund at Western University.

REFERENCES

- Aquilina A., Connelly D. P., Copley J. T., Green D. R. H., Hawkes J. A., Hepburn L. E., Huvenne V. A. I., Marsh L., Mills R. A. and Tyler P. A. (2013) Geochemical and visual indicators of hydrothermal fluid flow through a sediment-hosted volcanic ridge in the Central Bransfield Basin (Antarctica). *PLoS ONE* **8**(1), e54686.
- Arnorsson S., Gronvold K. and Sigurdsson S. (1978) Aquifer chemistry of four high-temperature geothermal systems in Iceland. *Geochim. Cosmochim. Acta* **42**(5), 523–536.
- Bear L. M. (1963) *The Mineral Resources and Mining Industry of Cyprus*. Cyprus Geological Survey Department, Nicosia, p. 208.
- Bendel V., Fouquet Y., Auzende J.-M., Lagabrielle Y., Grimaud D. and Urabe T. (1993) The White Lady hydrothermal field, North Fiji back-arc basin, Southwest Pacific. *Econ. Geol.* **88**, 2237–2249.
- Berndt M. E. and Seyfried W. E. (1990) Boron, bromine, and other trace elements as clues to the fate of chlorine in mid-ocean ridge vent fluids. *Geochim. Cosmochim. Acta* **54**, 2235–2245.
- Berndt M. E., Seyfried W. E. and Beck J. W. (1988) Hydrothermal alteration processes at mid-ocean ridges: experimental and theoretical constraints from Ca and Sr exchange reactions. *J. Geophys. Res.* **93**(B5), 4573–4583.
- Berndt M. E., Seal R. R., Shanks W. C. and Seyfried W. E. (1996) Hydrogen isotope systematics of phase separation in submarine hydrothermal systems: experimental calibration and theoretical models. *Geochim. Cosmochim. Acta* **60**(9), 1595–1604.
- Bischoff J. L. and Rosenbauer R. (1985) An empirical equation of state for hydrothermal seawater (3.2 percent NaCl). *Am. J. Sci.* **285**(8), 725–763.
- Bowers T. S. (1989) Stable isotope signatures of water–rock interaction in mid-ocean ridge hydrothermal systems: sulphur, oxygen and hydrogen. *J. Geophys. Res.* **94**(B5), 5775–5786.
- Bowers T. S. and Taylor H. P. (1985) An integrated chemical and stable-isotope model of the origin of mid-ocean ridge hot spring systems. *J. Geophys. Res.* **90**(B14), 12583–12606.
- Bruguier N. J. and Livermore R. A. (2001) Enhanced magma supply at the southern East Scotia Ridge: evidence for mantle flow around the subducting slab? *Earth Planet. Sci. Lett.* **191**, 129–144.
- Butterfield D. A. and Massoth G. J. (1994) Geochemistry of North Cleft Segment vent fluids—temporal changes in chlorinity and their possible relation to recent volcanism. *J. Geophys. Res.* **99**(B3), 4951–4968.
- Butterfield D. A., Massoth G. J., McDuff R. E., Lupton J. E. and Lilley M. D. (1990) Geochemistry of hydrothermal fluids from Axial Seamount Hydrothermal Emissions Study vent field, Juan de Fuca Ridge. *J. Geophys. Res.* **95**, 12895–12921.
- Butterfield D. A., McDuff R. E., Mottl M. J., Lilley M. D., Lupton J. E. and Massoth G. J. (1994) Gradients in the composition of hydrothermal fluids from the Endeavour Segment vent field: phase separation and brine loss. *J. Geophys. Res.* **99**(B5), 9561–9583.
- Butterfield D. A., Seyfried W. E. and Lilley M. D. (2003) Composition and evolution of hydrothermal fluids. In *Dahlem Workshop Report: Energy and Mass transfer in Hydrothermal Systems*, vol. 89 (eds. P. E. Halbach, V. Tunncliffe and J. R. Hein). Dahlem University Press, pp. 123–161.
- Butterfield D. A., Nakamura K., Takano B., Lilley M. D., Lupton J. E., Resing J. A. and Rose K. K. (2011) High SO_2 flux, sulphur accumulation, and gas fractionation at an erupting submarine volcano. *Geology* **39**, 803–806.
- Charlou J. L., Fouquet Y., Donval J. P. and Auzende J. M. (1996) Mineral and gas chemistry of hydrothermal fluids on an ultrafast spreading ridge: East Pacific Rise, 17° to 19°S (Naudur cruise, 1993) phase separation processes controlled by volcanic and tectonic activity. *J. Geophys. Res.* **101**, 15899–15919.
- Charlou J. L., Donval J. P., Douville E., Jean-Baptiste P., Radford-Knoery J., Fouquet Y., Dapigny A. and Stievenard M. (2000) Compared geochemical signatures and the evolution of Menez Gwen (37°50'N) and Lucky Strike (37°17'N) hydrothermal fluids, south of the Azores triple junction on the Mid-Atlantic Ridge. *Chem. Geol.* **171**, 345–359.
- Craig H. and Lupton J. E. (1981) Helium-3 and mantle volatiles in the ocean and ocean crust. In *The Sea, vol. 7: The Oceanic Lithosphere* (ed. C. Emiliani). Wiley, pp. 391–428.
- Edmond J. M., Measures C., McDuff R. E., Chan L. H., Collier R., Grant B., Gordon L. I. and Corliss J. B. (1979) Ridge crest hydrothermal activity and the balances of the major and minor elements in the ocean: the Galapagos data. *Earth Planet. Sci. Lett.* **46**, 1–18.
- Edmond J. M., Massoth G. and Lilley M. D. (1992) Submersible deployed samplers for axial vent waters. *RIDGE Events* **3**(1), 23–24.
- Edmond J. M., Campbell A. C., Palmer M. R., Kilnhammer G., German C. R., Edmonds H. N., Elderfield H., Thompson G. and Rona P. (1995) Time series studies of vent fluids from the TAG and MARK sites (1986, 1990) Mid-Atlantic Ridge: a new solution chemistry model and a mechanism for Cu/Zn zonation in massive sulphide ore bodies. In *Hydrothermal Vents and Processes* (eds. L. Parson and J. R. Dixon). Geological Society Special Publication No. 87, pp. 77–86.
- Edmonds H. N., German C. R., Green D. R. H., Huh Y., Gamo T. and Edmond J. M. (1996) Continuation of the hydrothermal fluid chemistry time series at TAG, and the effects of ODP drilling. *Geophys. Res. Lett.* **23**, 3487–3489.
- Eissen J.-P., Nohara M., Cotton J. and Hirose K. (1994) North Fiji Basin basalts and their magma sources: Part I. Incompatible element constraints. *Mar. Geol.* **116**, 153–178.
- Embley R. W., Chadwick W. W., Baker E. T., Butterfield D. A., Resing J. A., de Ronde C. E. J., Tunncliffe V., Lupton J. E., Juniper S. K., Rubin K. H., Stern R. J., Lebon G. T.,

- Nakamura Y., Merle S. G., Hein J. R., Wiens D. A. and Tamura Y. (2006) Long-term eruptive activity at a submarine arc volcano. *Nature* **441**, 494–497.
- Fouquet Y., Auclair G., Cambon P. and Etoubleu J. (1988) Geological setting and mineralogical and geochemical investigations on sulfide deposits near 13°N on the East Pacific Rise. *Mar. Geol.* **84**, 145–178.
- Fouquet Y., von Stackelberg U., Charlou J.-L., Erzinger J., Herzig P. M., Mühe R. and Wiedicke M. (1993) Metallogenesis in back-arc environments: the Lau Basin example. *Econ. Geol.* **88**, 2154–2181.
- Fournier R. O. (1983) A method of calculating quartz solubilities in aqueous sodium-chloride solutions. *Geochim. Cosmochim. Acta* **47**(3), 579–586.
- Foustoukos D. I. and Seyfried W. E. (2005) Redox and pH constraints in the subseafloor root zone of the TAG hydrothermal system, 26°N Mid-Atlantic Ridge. *Earth Planet. Sci. Lett.* **235**, 497–510.
- Foustoukos D. I. and Seyfried W. E. (2007a) Trace element partitioning between vapour, brine and halite under extreme phase separation conditions. *Geochim. Cosmochim. Acta* **71**(8), 2056–2071.
- Foustoukos D. I. and Seyfried W. E. (2007b) Quartz solubility in the two-phase and critical region of the NaCl–KCl–H₂O system: implications for submarine hydrothermal vent systems at 9°50'N East Pacific Rise. *Geochim. Cosmochim. Acta* **71**(1), 186–201.
- Foustoukos D. I. and Seyfried W. E. (2007c) Fluid phase separation processes in submarine hydrothermal systems. In *Fluid–Fluid Interactions*, vol. 65 (eds. A. Liebscher and C. A. Heinrich). Reviews in Mineralogy and Geochemistry. Mineralogical Society of America, pp. 213–239.
- Fretzdorff S., Livermore R. A., Devey C. W., Leat P. T. and Stoffers P. (2002) Petrogenesis of the back-arc East Scotia Ridge, South Atlantic Ocean. *J. Petrol.* **43**(8), 1435–1467.
- Gallant R. M. and Von Damm K. L. (2006) Geochemical controls on hydrothermal fluids from the Kairei and Edmond vent fields, 23–25°S, Central Indian Ridge. *Geochem. Geophys. Geosyst.* **7**, Q06018.
- Gamo T. (1995) Wide variation of chemical characteristics of submarine hydrothermal fluids due to secondary modification processes after high-temperature water–rock interaction: a review. In *Biogeochemical Processes and Ocean Flux in the Western Pacific* (eds. H. Sakai and Y. Nozaki). Terra Scientific Publishing, Tokyo, Japan, pp. 425–452.
- Gamo T., Okamura K., Charlou J.-L., Urabe T., Auzende J.-M., Ishibashi J.-I., Shitashima K. and Chiba H. and the Shipboard Scientific Party of the ManusFlux Cruise (1997) Acidic and sulphate-rich hydrothermal fluids from the Manus back-arc basin, Papua New Guinea. *Geology* **25**(2), 139–142.
- Gamo T., Ishibashi J.-I., Tsunogai U., Okamura K. and Chiba H. (2006) Unique geochemistry of submarine hydrothermal fluids from back-arc settings of the western Pacific. In *Back-Arc Spreading Systems: Geological, Biological, Chemical and Physical Interactions*. Geophysical Monograph Series 166 (eds. D. M. Christie, C. R. Fisher, S. -M., Lee and S. Givens). American Geophysical Union, pp. 147–161.
- German C. R., Livermore R. A., Baker E. T., Bruguier N. I., Connelly D. P., Cunningham A. P., Morris P., Rouse I. P., Statham P. J. and Tyler P. A. (2000) Hydrothermal plumes above the East Scotia Ridge: an isolated high-latitude back-arc spreading centre. *Earth Planet. Sci. Lett.* **184**, 241–250.
- German C. R. and Von Damm K. L. (2003) Hydrothermal processes. In *Treatise on Geochemistry*, vol. 6 (eds. K. K. Turekian and H. D. Holland). Elsevier, pp. 181–222.
- Graham U. M., Bluth G. J. and Ohmoto H. (1988) Sulfide-sulfate chimneys on the East Pacific Rise, 11°N and 13°N Latitudes, I. Mineralogy and paragenesis. *Can. Mineral.* **26**, 487–504.
- Grimaud D., Ishibashi J., Lagabrielle Y., Auzende J.-M. and Urabe T. (1991) Chemistry of hydrothermal fluids from the 17°S active site on the North Fiji Basin Ridge (SW Pacific). *Chem. Geol.* **93**, 209–218.
- Harvey-Kelly F. E. L., Jonnason I. R., Franklin J. M. and Embley R. W. (1988) Sulfide deposits on Axial Seamount: mineralogy and chemistry. *EOS Trans. Am. Geophys. Union* **69**, 1499.
- Haymon R. (1983) Growth history of hydrothermal black smoker chimneys. *Nature* **301**, 695–698.
- Ishibashi J. and Urabe T. (1995) Hydrothermal activity related to back-arc magmatism in the western Pacific. In *Backarc Basins: Tectonics and Magmatism* (ed. B. Taylor). Plenum Press, New York, pp. 451–495.
- Ishibashi J., Grimaud D., Nojiri Y., Auzende J.-M. and Urabe T. (1994) Fluctuation of chemical compositions of the phase-separated hydrothermal fluids from the North Fiji Basin Ridge. *Mar. Geol.* **116**, 215–226.
- Ito E., White W. M. and Göpel C. (1987) The O, Sr, Nd and Pb isotope geochemistry of MORB. *Chem. Geol.* **62**, 157–176.
- James R. H., Elderfield H. and Palmer M. R. (1995) The chemistry of hydrothermal fluids from the Broken Spur site, 29°N Mid-Atlantic Ridge. *Geochim. Cosmochim. Acta* **59**, 651–659.
- Kakegawa T., Utsumi M. and Marumo K. (2008) Geochemistry of sulphide chimneys and basement pillow lavas at the Southern Mariana Trough (12.55°N–12.58°N). *Res. Geol.* **58**, 249–266.
- Kato S., Nakamura K., Toki T., Ishibashi J.-I., Tsunogai U., Hirota A., Ohkuma M. and Yamagishi A. (2012) Iron-based microbial ecosystem on and below the seafloor: a case study of hydrothermal fields of the Southern Mariana Trough. *Front. Microbiol.* **3**, Article 89.
- Kawagucci S., Chiba H., Ishibashi J.-I., Yamanaka T., Toki T., Muramatsu Y., Ueno Y., Makabe A., Inoue K., Yoshida N., Nakagawa S., Nunoura T., Takai K., Takahata N., Sano Y., Narita T., Ternaishi G., Obata H. and Gamo T. (2011) Hydrothermal fluid chemistry at the Iheya North field in the mid-Okinawa Trough: Implication for origin of methane in subseafloor circulation systems. *Geochem. J.* **45**, 109–124.
- Kawagucci S., Ueno Y., Takai K., Toki T., Ito M., Inoue K., Makabe A., Yoshida N., Muramatsu Y., Takahata N., Sano Y., Narita T., Ternaishi G., Obata H., Nakagawa S., Nunoura T. and Gamo T. (2013) Geochemical origin of hydrothermal fluid methane in sediment-associated fields and its relevance to the geographical distribution of whole hydrothermal system. *Chem. Geol.* **339**, 213–225.
- Koschinsky A., Garbe-Schönberg D., Sander S., Schmidt K., Gennerich H.-H. and Strauss H. (2008) Hydrothermal venting at pressure–temperature conditions above the critical point of seawater, 5°S on the Mid-Atlantic Ridge. *Geology* **36**, 615–618.
- Koski R. A., Lonsdale P. F., Shanks W. C., Berndt M. E. and Howe S. S. (1985) Mineralogy and geochemistry of a sediment-hosted hydrothermal sulfide deposit from the southern trough of Guaymas Basin, Gulf of California. *J. Geophys. Res.* **90**, 6695–6707.
- Koski R. A., Jonasson I. R., Kadko D. C., Smith V. K. and Wong F. L. (1994) Compositions, growth mechanisms, and temporal relations of hydrothermal sulfide-sulfate-silica chimneys at the northern Cleft segment, Juan de Fuca Ridge. *J. Geophys. Res.* **99**(B3), 4813–4832.
- Klinkhammer G. P., Chin C. S., Keller R. A., Dählmann A., Sahling H., Sarthou G., Petersen S. and Smith F. (2001) Discovery of new hydrothermal vent sites in Bransfield Strait, Antarctica. *Earth Planet. Sci. Lett.* **193**(1–4), 395–407.

- Kumagai H., Nakamura K., Toki T., Morishita T., Okino K., Ishibashi J.-I., Tsunogai U., Kawagucci S., Gamo T., Shibuya T., Sawaguchi T., Neo N., Joshima M., Sata T. and Takai K. (2008). *Geofluids* **8**, 239–251.
- Larter R. D., Vanneste L. E., Morris P. and Smyth D. K. (2003) Tectonic evolution and structure of the South Sandwich arc. In *Intra-Oceanic Subduction Systems: Tectonic and Magmatic Processes* (eds. R. D. Larter and P. T. Leat). Geol. Soc. London Spec. Publ. 219, pp. 255–284.
- Leat P. T., Livermore R. A., Millar I. L. and Pearce J. A. (2000) Magma supply in back-arc spreading centre segment E2, East Scotia Ridge. *J. Petrol.* **41**, 845–866.
- Leat P. T., Pearce J. A., Barker P. F., Millar I. L., Barry T. L. and Larter R. D. (2004) Magma genesis and mantle flow at a subducting slab edge: the South Sandwich arc-basin system. *Earth Planet. Sci. Lett.* **227**, 17–35.
- Liebscher A., Lüders V., Heinrich W. and Schettler G. (2006) Br/Cl signature of hydrothermal fluids: liquid–vapour fractionation of bromine revisited. *Geofluids* **6**, 113–121.
- Livermore R., Cunningham A., Vanneste L. and Larter R. (1997) Subduction influence of magma supply at the East Scotia Ridge. *Earth Planet. Sci. Lett.* **150**, 261–275.
- Lupton J., Butterfield D., Lilley M., Evans L., Nakamura K., Chadwick W., Resing J., Embley R., Olson E., Proskurowski G., Baker E., de Ronde C., Roe K., Greene R., Lebon G. and Young C. (2006) Submarine venting of liquid carbon dioxide on a Mariana Arc volcano. *Geochem. Geophys. Geosyst.* **7**(8), Q08007.
- Maris C. R. P., Bender M. L., Froelich P. N., Barnes R. and Luedtke N. A. (1984) Chemical evidence for advection of hydrothermal solutions in the sediments of the Galápagos mounds hydrothermal field. *Geochim. Cosmochim. Acta* **48**(11), 2331–2346.
- Marsh L., Copley J. T., Huvenne V. A. I., Linse K., Reid W. D. K., Rogers A. D., Sweeting C. J. and Tyler P. A. (2012) Micro-distribution of faunal assemblages at the deep-sea hydrothermal vents in the Southern Ocean. *PLoS ONE* **7**(10), e48348.
- Marty B. and Jambon A. (1987) C^3He in volatile fluxes from the solid Earth: implications for carbon geodynamics. *Earth Planet. Sci. Lett.* **83**, 16–26.
- Mills R. A. and Elderfield H. (1995) Rare earth element geochemistry of hydrothermal deposits from the active Tag Mound, 26°N Mid-Atlantic Ridge. *Geochim. Cosmochim. Acta* **59**(17), 3511–3524.
- Moore W. S. and Stakes D. (1990) Ages of barite-sulfide chimneys from the Mariana Trough. *Earth Planet. Sci. Lett.* **100**, 265–274.
- Mottl M. J. and Holland H. D. (1978) Chemical exchange during hydrothermal alteration of basalt by seawater: I. Experimental results for major and minor components of seawater. *Geochim. Cosmochim. Acta* **42**(8), 1103–1115.
- Mottl M. J., Seewald J. S., Wheat C. G., Tivey M. K., Michael P. J., Proskurowski G., McCollom T. M., Reeves E., Sharkey J., You C.-F., Chan L.-H. and Pichler T. (2011) Chemistry of hot springs along the Eastern Lau Spreading Centre. *Geochim. Cosmochim. Acta* **75**, 1013–1038.
- Nakagawa S., Takai K., Inagaki F., Chiba H., Ishibashi J.-I., Kataoka S., Hirayama H., Nunoura T., Horikoshi K. and Sako Y. (2005) Variability in microbial community and venting chemistry in a sediment-hosted backarc hydrothermal system: impacts of seafloor phase-separation. *FEMS Microbiol. Ecol.* **54**, 141–155.
- Nakamura K., Morishita T., Bach W., Klein F., Hara K., Okino K., Takai K. and Kumagai H. (2009) Serpentinized troctolites exposed near the Kairei hydrothermal field, Central Indian Ridge: Insights into the origin of the Kairei hydrothermal fluid supporting a unique microbial ecosystem. *Earth Planet. Sci. Lett.* **280**, 128–136.
- Nakamura K., Toki T., Mochizuki N., Asada M., Ishibashi J.-I., Nogi Y., Yoshikawa S., Miyazaki J.-I. and Okino K. (2013) Discovery of a new hydrothermal vent based on an underwater, high-resolution geophysical survey. *Deep-Sea Res.* **174**, 1–10.
- Ohmoto H. (1986) Stable isotope geochemistry of ore deposits. In *Stable Isotopes in High Temperature Geological Processes*, vol. 16 (eds. J. W. Valley, H. P. Taylor and J. R. O'Neill). Reviews in Mineralogy. Mineralogical Society of America, pp. 491–559.
- Pearce J. A. and Peate D. W. (1995) Tectonic implications of the composition of volcanic arc magmas. *Annu. Rev. Earth Planet. Sci. Lett.* **23**, 251–285.
- Pearce J. A. and Robinson P. T. (2010) The Troodos ophiolitic complex probably formed in a subduction initiation, slab edge setting. *Gondwana Res.* **18**, 60–81.
- Pearce J. A., Ernewein M., Bloomer S. H., Parson L. M., Murton B. J. and Johnson L. E. (1995) Geochemistry of Lau Basin volcanic rocks: influence of ridge segmentation and arc proximity. In *Volcanism Associated with Extension at Consuming Plate Margins* (ed. J. L. Smellie). Geol. Soc. London Spec. Publ. 81, pp. 53–75.
- Peccerillo A. and Taylor S. R. (1976) Geochemistry of Eocene calc-alkaline volcanic rocks from the Kastamonu area, northern Turkey. *Contrib. Mineral. Petrol.* **58**, 63–81.
- Powell A. P., Banerjee N. R., Munro L. E., Hisao G. and James R. H. (2011) Investigations of deep-sea hydrothermal samples for isotopic composition and interfering compounds using CRDS. *IAEA International Symposium on Stable Isotopes in Hydrology, Marine Ecosystems and Climate Change Studies*, Oceanographic Museum of Monaco, 27 March – 1 April 2011.
- Reeves E. P., Seewald J. S., Saccocia P., Bach W., Craddock P. R., Shanks W. C., Sylva S. P., Walsh E., Pichler T. and Rosner M. (2011) Geochemistry of hydrothermal fluids from the PACMANUS, Northeast Pual and Vienna Woods hydrothermal fields, Manus Basin, Papua New Guinea. *Geochim. Cosmochim. Acta* **75**, 1088–1123.
- Rogers A. D., Tyler P. A., Connelly D. P., Copley J. T., James R., Larter R. D., Linse K., Mills R. A., Naveira Garabato A., Pancost R. D., Pearce D. A., Polunin N. V. C., German C. R., Shank T., Boersch-Supan P. H., Alker B. J., Aquilina A., Bennett S. A., Clarke A., Dinley R. J. J., Graham A. G. C., Green D. R. H., Hawkes J. A., Hepburn L., Hilario A., Huvenne V. A. I., Marsh M., Ramirez-Llodra E., Reid W. D. K., Roterman C. N., Sweeting C. J., Thatje S. and Zwirgmaier Z. (2012) The discovery of new deep-sea hydrothermal vent communities in the Southern Ocean and implications for biogeography. *PLoS Biol.* **10**(1), e1001234.
- Ryan J. G. and Langmuir C. H. (1987) The systematic of lithium abundances in young volcanic rocks. *Geochim. Cosmochim. Acta* **51**, 1727–1741.
- Ryan J. G. and Langmuir C. H. (1993) The systematics of boron abundances in young volcanic rocks. *Geochim. Cosmochim. Acta* **57**, 1489–1498.
- Schmidt K., Garbe-Schönberg D., Koschinsky A., Strauss H., Jost C. L., Klevenz V. and Königer P. (2011) Fluid elemental and stable isotope composition of the Nibelungen hydrothermal field (8°18'S, Mid-Atlantic Ridge): constraints on fluid–rock interaction in heterogeneous lithosphere. *Chem. Geol.* **280**, 1–18.
- Sedwick P. N., McMurtry G. M., Hilton D. R. and Goff F. (1994) Carbon dioxide and helium in hydrothermal fluids from Loihi Seamount, Hawaii, USA: temporal variability and implications for release of magmatic volatiles. *Geochim. Cosmochim. Acta* **58**(3), 1219–1227.

- Seewald J. S. and Seyfried W. E. (1990) The effect of temperature on metal mobility in seafloor hydrothermal systems: constraints from basalt alteration experiments. *Earth Planet. Sci. Lett.* **101**, 388–403.
- Seewald J., Cruse A. and Saccoccia P. (2003) Aqueous volatiles in hydrothermal fluids from the Main Endeavour Field, northern Juan de Fuca Ridge: temporal variability following earthquake activity. *Earth Planet. Sci. Lett.* **216**(4), 575–590.
- Seyfried W. E. and Ding K. (1993) The effect of redox on the relative solubilities of copper and iron in Cl-bearing aqueous fluids at elevated temperatures and pressures: an experimental study with application to seafloor hydrothermal systems. *Geochim. Cosmochim. Acta* **57**, 1905–1917.
- Seyfried W. E. and Ding K. (1995) The hydrothermal chemistry of fluoride in seawater. *Geochim. Cosmochim. Acta* **59**(6), 1063–1071.
- Seyfried W. E., Seewald J. S., Berndt M. E., Ding K. and Foustoukos D. (2003) Chemistry of hydrothermal vent fluids from the main Endeavour Field, northern Juan de Fuca Ridge: geochemical controls in the aftermath of the June 1999 seismic events. *J. Geophys. Res.* **108**, 2429–2452.
- Shanks W. C. (2001) Stable isotopes in seafloor hydrothermal systems: vent fluids, hydrothermal deposits, hydrothermal alteration, and microbial processes. In *Stable Isotope Geochemistry*, vol. 43 (eds. J. W. Valley and D. R. Cole). Reviews in Mineralogy & Geochemistry. Mineralogical Society of America, pp. 469–525.
- Shanks W. V., Böhlke J. K. and Seal R. R. (1995) Stable isotopes in mid-ocean ridge hydrothermal systems: interactions between fluids, minerals, and organisms. In *Seafloor Hydrothermal Systems: Physical, Chemical, Biological and Geological Interactions*, vol. 91 (eds. S. E. Humphris, R. A. Zierenberg, L. S. Mullineaux and R. E. Thompson). AGU Monograph. American Geophysical Union, pp. 194–221.
- Shinjo R., Chung S.-L., Kato Y. and Kimura M. (1999) Geochemical and Sr–Nd isotopic characteristics of volcanic rocks from the Okinawa Trough and Ryukyu Arc: implications for the evolution of a young, intracontinental back arc basin. *J. Geophys. Res.* **104**, 10591–10608.
- Sinton J. M., Ford L. L., Chappell B. and McCulloch M. T. (2003) Magma genesis and mantle heterogeneity in the Manus back-arc basin, Papua New Guinea. *J. Petrol.* **44**, 159–195.
- Spivack A. J. and Edmond J. M. (1987) Boron isotope exchange between seawater and the oceanic crust. *Geochim. Cosmochim. Acta* **51**, 1033–1043.
- Strickland J. D. H. and Parsons T. R. (1968) *A Practical Handbook of Seawater Analysis*. Fisheries Research Board of Canada, Bulletin 167, 293 pp.
- Suzuki R., Ishibashi J.-I., Nakaseama M., Konno U., Tsunogai U., Gena K. and Chiba H. (2008) Diverse range of mineralization induced by phase separation of hydrothermal fluid: case study of the Yonaguni Knoll IV hydrothermal field in the Okinawa Trough back-arc basin. *Res. Geol.* **58**, 267–288.
- Taylor H. P. (1979) Oxygen and hydrogen isotope relationships in hydrothermal mineral deposits. In *Geochemistry of Hydrothermal Ore Deposits* (ed. H. L. Barnes). Wiley, pp. 299–302.
- Tian L., Zhao G., Zhao G., Shi X. and Hailong L. (2005) Geochemistry of basaltic lavas from the Mariana Trough: evidence for influence of subduction component on the generation of backarc basin magmas. *Int. Geol. Rev.* **47**, 387–397.
- Tivey M. K. (1995) The influence of hydrothermal fluid composition and advection rates on black smoker chimney mineralogy: insights from modelling transport and reaction. *Geochim. Cosmochim. Acta* **59**(10), 1933–1949.
- Von Damm K. L. (1990) Seafloor hydrothermal activity: black smoker chemistry and chimneys. *Annu. Rev. Earth Planet. Sci.* **18**, 173–204.
- Von Damm K. L. (1995) Controls on the chemistry and temporal variability of seafloor hydrothermal systems. In *Seafloor Hydrothermal Systems: Physical, Chemical, Biological and Geological Interactions*, vol. 91 (eds. S. E. Humphris, R. A. Zierenberg, L. S. Mullineaux and R. E. Thompson). AGU Monograph. American Geophysical Union, pp. 222–247.
- Von Damm K. L. (2000) Chemistry of hydrothermal vent fluids from 9–10°N, East Pacific Rise: ‘Time zero’, the immediate post-eruptive period. *J. Geophys. Res.* **105**(B5), 11203–11222.
- Von Damm K. L. and Bischoff J. L. (1987) Chemistry of hydrothermal solutions from the Southern Juan de Fuca Ridge. *J. Geophys. Res.* **92**, 11334–11346.
- Von Damm K. L., Edmond J. M., Grant B. and Measures C. I. (1985) Chemistry of submarine hydrothermal solutions at 21°N, East Pacific Rise. *Geochim. Cosmochim. Acta* **49**(11), 2197–2220.
- Von Damm K. L., Bischoff J. L. and Rosenbauer R. J. (1991) Quartz solubility in hydrothermal seawater: an experimental study and equation describing quartz solubility for up to 0.5 M NaCl solutions. *Am. J. Sci.* **291**(10), 977–1007.
- Von Damm K. L., Buttermore L. G., Oosting S. E., Bray A. M., Fornari D. J., Lilley M. D. and Shanks W. C. (1997) Direct observation of the evolution of a seafloor ‘blank smoker’ from vapour to brine. *Earth Planet. Sci. Lett.* **149**(1–4), 101–111.
- Von Damm K. L., Lilley M. D., Shanks W. C., Brockington M., Bray A. M., O’Grady K. M., Olson E., Graham A. and Proskurowski G. and the SouEPR Science Party (2003) Extraordinary phase separation and segregation in vent fluids from the southern East Pacific Rise. *Earth Planet. Sci. Lett.* **206**, 365–378.
- You C.-F., Butterfield D. A., Spivack A. J., Gieskes J. M., Gamo T. and Campbell A. J. (1994) Boron and halide systematics in submarine hydrothermal systems: effects of phase separation and sedimentary contributions. *Earth Planet. Sci. Lett.* **123**, 227–238.

Associate editor: Jeffrey C. Alt